

11-2016

Version 1.3 AIM SOFIE Measured Methane (CH₄): Validation and Seasonal Climatology

P. P. Rong

J. M. Russell III


B. T. Marshall

D. E. Siskind

M. E. Hervig

See next page for additional authors

Follow this and additional works at: https://digitalcommons.odu.edu/chemistry_fac_pubs

 Part of the [Atmospheric Sciences Commons](#), [Chemistry Commons](#), [Climate Commons](#), and the [Meteorology Commons](#)

Repository Citation

Rong, P. P.; Russell, J. M. III; Marshall, B. T.; Siskind, D. E.; Hervig, M. E.; Gordley, L. L.; Bernath, P. F.; and Walker, K. A., "Version 1.3 AIM SOFIE Measured Methane (CH₄): Validation and Seasonal Climatology" (2016). *Chemistry & Biochemistry Faculty Publications*. 61.

https://digitalcommons.odu.edu/chemistry_fac_pubs/61

Original Publication Citation

Rong, P. P., Russell, J. M., III, Marshall, B. T., Siskind, D. E., Hervig, M. E., Gordley, L. L., . . . Walker, K. A. (2016). Version 1.3 AIM SOFIE measured methane (CH₄): Validation and seasonal climatology. *Journal of Geophysical Research: Atmospheres*, 121(21), 13,158-113,179. doi:10.1002/2016JD025415

Authors

P. P. Rong, J. M. Russell III, B. T. Marshall, D. E. Siskind, M. E. Hervig, L. L. Gordley, P. F. Bernath, and K. A. Walker

RESEARCH ARTICLE

10.1002/2016JD025415

Key Points:

- SOFIE CH₄ agrees qualitatively well with ACE and MIPAS CH₄ in vertical distribution and variability
- SOFIE CH₄ is biased high by ~20% in the lower stratosphere below ~25 km and is biased low by a similar percentage above ~65 km
- SOFIE CH₄ and MLS H₂O provide details on the 2CH₄ + H₂O balance in the polar stratosphere throughout a year

Correspondence to:

P. P. Rong,
ppr@jhu.edu

Citation:

Rong, P. P., J. M. Russell III, B. T. Marshall, D. E. Siskind, M. E. Hervig, L. L. Gordley, P. F. Bernath, and K. A. Walker (2016), Version 1.3 AIM SOFIE measured methane (CH₄): Validation and seasonal climatology, *J. Geophys. Res. Atmos.*, 121, 13,158–13,179, doi:10.1002/2016JD025415.

Received 24 MAY 2016

Accepted 18 OCT 2016

Accepted article online 20 OCT 2016

Published online 10 NOV 2016

Version 1.3 AIM SOFIE measured methane (CH₄): Validation and seasonal climatology

P. P. Rong¹, J. M. Russell III¹, B. T. Marshall², D. E. Siskind³, M. E. Hervig⁴, L. L. Gordley², P. F. Bernath⁵, and K. A. Walker⁶

¹Center for Atmospheric Sciences, Hampton University, Hampton, Virginia, USA, ²GATS, Inc., Newport News, Virginia, USA, ³Naval Research Laboratory, Washington, District of Columbia, USA, ⁴GATS, Inc., Driggs, Idaho, USA, ⁵Department of Chemistry & Biochemistry, Old Dominion University, Norfolk, Virginia, USA, ⁶Department of Physics, University of Toronto, Toronto, Ontario, Canada

Abstract The V1.3 methane (CH₄) measured by the Aeronomy of Ice in the Mesosphere (AIM) Solar Occultation for Ice Experiment (SOFIE) instrument is validated in the vertical range of ~25–70 km. The random error for SOFIE CH₄ is ~0.1–1% up to ~50 km and degrades to ~9% at ~70 km. The systematic error remains at ~4% throughout the stratosphere and lower mesosphere. Comparisons with CH₄ data taken by the SCISAT Atmospheric Chemistry Experiment-Fourier Transform Spectrometer (ACE-FTS) and the Envisat Michelson Interferometer for Passive Atmospheric Sounding (MIPAS) show an agreement within ~15% in the altitude range ~30–60 km. Below ~25 km SOFIE CH₄ is systematically higher (≥20%), while above ~65 km it is lower by a similar percentage. The sign change from the positive to negative bias occurs between ~55 km and ~60 km (or ~40 km and ~45 km) in the Northern (or Southern) Hemisphere. Methane, H₂O, and 2CH₄ + H₂O yearly differences from their values in 2009 are examined using SOFIE and MIPAS CH₄ and the Aura Microwave Limb Sounder (MLS) measured H₂O. It is concluded that 2CH₄ + H₂O is conserved with altitude up to an upper limit between ~35 km and ~50 km depending on the season. In summer this altitude is higher. In the Northern Hemisphere the difference relative to 2009 is the largest in late spring and the established difference prevails throughout summer and fall, suggesting that summer and fall are dynamically quiet. In both hemispheres during winter there are disturbances (with a period of ~1 month) that travel downward throughout the stratosphere with a speed similar to the winter descent.

1. Introduction

Methane (CH₄) is well mixed vertically in the troposphere, reaching about ~1.5–2.0 parts per million by volume (ppmv), and then rapidly decreases to 0.1 ppmv or smaller above the stratopause. There is no source of CH₄ in the atmosphere, and all the emissions come from the Earth's surface from processes such as organic matter decomposition and fossil fuel burning. Anthropogenic sources, such as natural gas combustion, industrial mining, landfills, and other processes, contribute nearly 70% of the total CH₄ release into the atmosphere [Brasseur and Solomon, 2005]. Although the CH₄ abundance in the troposphere is much lower than that of carbon dioxide (CO₂) or water vapor (H₂O), it is one of the most potent greenhouse gases in the atmosphere [e.g., Lashof and Ahuja, 1990; Howarth, 2015]. Therefore, understanding the CH₄ budget throughout the atmosphere is important to assess its potential effect on climate change.

Methane destruction in the stratosphere and lower mesosphere is due to reactions with the hydroxyl radical (OH), excited oxygen O(¹D), and chlorine atoms (Cl) [Brasseur and Solomon, 2005]. Methane oxidation proceeds largely through forming the partially oxygenated organic compound formaldehyde (CH₂O). Formaldehyde oxidizes through reaction with OH to produce H₂O. Photolysis of CH₂O also produces hydrogen radicals that recombine to produce H₂O. Methane destruction via this long chain reaction eventually produces H₂O and H₂ in the stratosphere and mesosphere, such that the sum of the hydrogen volume mixing ratio (vmr) 4CH₄ + 2H₂O + 2H₂ is approximately constant with altitude (neglecting other much less abundant hydrogen species such as OH and H). Since molecular hydrogen has a small mixing ratio (~0.6 ppmv), has a long photochemical lifetime (months to years), and remains roughly constant up to ~50 km altitude [Harries et al., 1996; Brasseur and Solomon, 2005], 2CH₄ + H₂O is often used to examine the hydrogen balance in the stratosphere and lower mesosphere. A nearly constant level of H₂ is maintained up to ~50 km because the rate at which H₂ is produced from CH₄ oxidation is coincidentally close to the rate of H₂ oxidation into

H₂O below ~60 km [Le Texier *et al.*, 1988]. The 2CH₄ + H₂O is also called “potential H₂” by Summers *et al.* [1997] because it represents the reservoir for the total hydrogen budget. The UARS Halogen Occultation Experiment (HALOE) [Russell *et al.*, 1993] data analysis and chemical model results both indicate that 2CH₄ + H₂O is conserved below ~50 km [Harries *et al.*, 1996; Summers *et al.*, 1997]. The increasing H₂O in the upper stratosphere can be qualitatively explained by the mechanism of CH₄ conversion to H₂O. The conversion is the strongest at the stratopause because rates of CH₂O oxidation and photolysis roughly maximize between ~30 km and ~50 km [Le Texier *et al.*, 1988]. Methane destruction by radicals and atoms is significantly weakened above the stratopause where photolysis of CH₄ by Lyman α irradiation becomes more significant [e.g., Minschwaner and Manney, 2014]. However, since the amount of CH₄ is increasingly small toward the upper part of the middle atmosphere, photolysis has a negligible impact on the total CH₄ budget [Brasseur and Solomon, 2005]. Due to its generally long photochemical time, CH₄ can be used as a tracer of transport throughout the stratosphere and mesosphere in many cases, although its validity as a tracer depends on the efficiency of chemical destruction. For example, low CH₄ and high nitric oxide (NO) were both used as tracers to show the effects of strong descent from ~90 km down to ~30 km altitude in the 2003–2004 polar winter to spring following the severe solar storm that occurred during Halloween 2003 [Randall *et al.*, 2005]. Similar analyses have been applied to other years with relatively significant descent such as in 1991, 2006, 2009, and the 2013 Northern Hemisphere (NH) polar winter-to-spring period [e.g., Siskind *et al.*, 2000; Bailey *et al.*, 2014; Funke *et al.*, 2014]. Overall, the vertical distribution of CH₄ is governed by the competition and eventual balance between chemical destruction and vertical and/or horizontal transport.

The Solar Occultation for Ice Experiment (SOFIE) [Gordley *et al.*, 2009] is one of two instruments currently operating aboard the Aeronomy of Ice in the Mesosphere (AIM) satellite (2007 to present) [Russell *et al.*, 2009]. The primary AIM mission goal is to study the polar mesospheric clouds (PMCs) [Hervig *et al.*, 2009; McClintock *et al.*, 2009], but the SOFIE level 2 products also include vertical profiles of temperature, H₂O, CH₄, O₃, NO, and CO₂ in the stratosphere and mesosphere. Aside from PMC studies, these constituents play important roles in atmospheric chemistry and dynamics. The SOFIE payload includes 16 broadband radiometers to measure vertical profiles of limb path atmospheric transmission in eight channels (or band pairs) ranging from the visible to short-to-medium infrared spectral range of 0.29–5.32 μm . Occultation measurements are accomplished by monitoring solar intensity as the satellite enters or exits the Earth's shadow (spacecraft sunrise or sunset). AIM is in a near-circular, ~595–601 km altitude, polar (97.8°) Sun-synchronous orbit, with a midnight/noon equator crossing. As a result, sunrise and sunset measurements occur exclusively in high-latitude regions. Due to the Earth obliquity, SOFIE latitude coverage varies moderately with season between 66°N/S and 83°N/S during the years (2008–2012) used in this study.

Figure 1a presents the SOFIE PMC extinction coefficient spectrum modeled assuming a Gaussian (cloud) particle size distribution, with the SOFIE band pairs overlapped shown as circles. Signals are received from both weak and strong bands. The band pair differences are used to improve the accuracy of the retrievals because a variety of solar, atmospheric, and instrumental effects are nearly equal and positively correlated in the strong and weak bands and therefore removed by electronically differencing the band pairs [Gordley *et al.*, 2009]. The main methane absorption bands used by SOFIE are centered at 3.384 μm and 3.479 μm and occur where the PMC extinction is at a moderate level compared to that in the O₃ channel (1) or H₂O channel (3) which is either large or negligibly small. Figure 1b shows the atmospheric limb transmission spectra at ~74 km for different species that contribute to the absorption in the CH₄ channel. It shows that the in-band interference from ozone and water vapor are both small. The PMC contamination is not shown among these curves, but the analysis is available at the SOFIE website which verifies that the impact can reach altitudes significantly lower than the centroid height of the PMC region (~83 \pm 1 km). The quantified PMC impact on different constituents is listed in full at <http://sofie.gats-inc.com/sofie/index.php> where channel characteristics are described. These online figures suggest that the SOFIE CH₄ product will not be very useful above ~70 km due to substantial contamination from the PMC signals. In this paper two correlative data sets, SCISAT Atmospheric Chemistry Experiment-Fourier Transform Spectrometer (ACE-FTS) Version 3.5 [Bernath *et al.*, 2005] and Envisat Michelson Interferometer for Passive Atmospheric Sounding (MIPAS) European Space Agency (ESA) reprocessed Version 6 [Raspollini *et al.*, 2006; Payan *et al.*, 2009; Engel *et al.*, 2016], are used to validate the SOFIE CH₄ results. Methane measurements from both spaceborne satellite missions and ground-based campaigns are generally lacking especially in the vertical range of >30 km where SOFIE

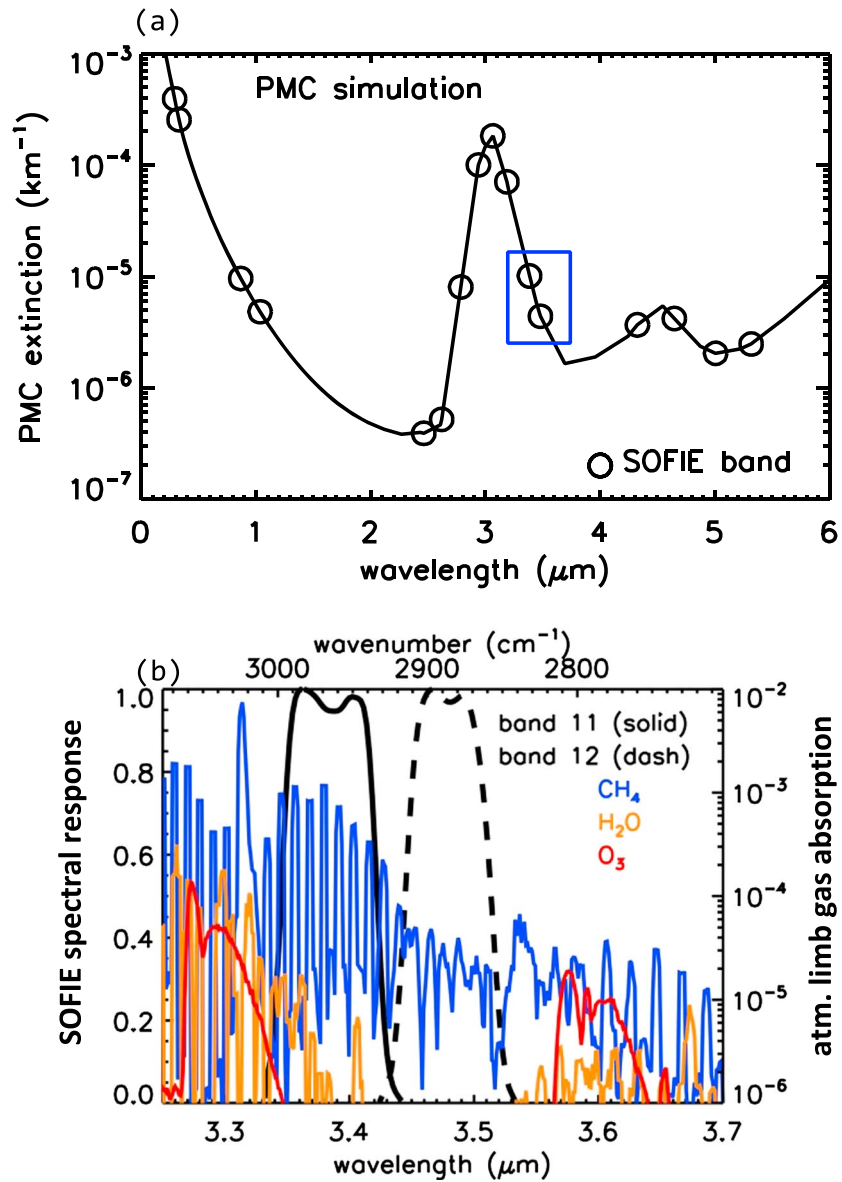


Figure 1. (a) SOFIE PMC extinction coefficient spectrum assuming a Gaussian size distribution. The circles are SOFIE band pairs. Methane is measured using the channel 6 pair (enclosed in the blue rectangle) centered at 3.384 μm and 3.479 μm for strong (solid black curve in Figure 1b) and weak (dashed black curve in Figure 1b) bands for CH_4 , respectively. (b) SOFIE spectral response for different species in the CH_4 bandpass spectral region.

CH_4 has the best data quality. ACE-FTS and MIPAS are two primary data sets that provide CH_4 products throughout the stratosphere and mesosphere up to ~ 70 km and have data coverages concurrent with SOFIE. In section 2 the SOFIE retrieval, error analysis, and the correlative data sets are introduced. Comparisons of the coincident pairs of vertical profiles are carried out in section 3. In section 4 CH_4 and H_2O seasonal climatology is discussed. Furthermore, the interannual variability and hemispheric differences of $2\text{CH}_4 + \text{H}_2\text{O}$ balance are explored using the differences relative to the 2009 distribution. Conclusions are given in section 5.

2. SOFIE Retrieval, Error Analysis, and Correlative Data Sets

2.1. SOFIE Retrieval and the CH_4 Error Analysis

SOFIE measures vertical profiles of limb atmospheric transmission, defined as the ratio of solar intensity measured through the atmosphere to the value measured outside the atmosphere. The BandPak forward model

Table 1. SOFIE Measurement Error Responses Determined Using Retrieval Simulations Based On a Presumed "True" State^a

Error Type	Altitude (km)				
	30	40	50	60	70
SOFIE random (%)	0.1	0.3	1	3	9
Forward	3.5	3.3	3.2	3.1	3.1
Interfering	1.9	1.8	1	0.3	0.1
Temperature	0.2	0.2	0.4	0.8	1.5
FOV	1	0.9	0.9	0.9	1
Registration	1.5	1.5	1.5	1.5	1.5
SOFIE total systematic (%)	4.38	4.15	3.80	3.66	3.89
SOFIE total	4.38	4.16	3.93	4.73	9.80

^aThe SOFIE CH₄ random error refers to the model-simulated response to the estimated measurement noise. The individual systematic error sources are detailed in section 2.1 of the paper. The total systematic error is the root-sum-square (RSS) of previous five error mechanisms. Total error is the RSS of systematic and random errors.

[Marshall *et al.*, 1994] is used to simulate the observed transmission for a given spectral band [Gordley *et al.*, 2009], and an "onion peeling" algorithm is used to carry out the retrievals assuming that the atmosphere is horizontally isothermal and evenly mixed within the limb path tangent layer (~300 km). A broadband forward model, such as the BandPak, could lead to much smaller systematic errors than a line-by-line model since systematic uncertainty of choosing microwindows is reduced. In this case, the errors are pseudorandom across the lines enveloped in the given broadband. The SOFIE instrument design provides an extremely high signal-to-noise ratio (SNR) of ~10⁵. The vertical resolution of all SOFIE level 2 products is ~2 km throughout their valid vertical ranges. The SOFIE data vertical spacing, however, is consistently 0.2 km. This is due to the fact that an interleave method [e.g., Remsberg *et al.*, 2008] is applied, in which case multiple retrievals with vertical spacing of ~2 km are combined to produce one final profile. Multiple retrievals within a ~2 km altitude distance are possible because single ray simulations are performed for various view angles within the field of view (FOV) [Gordley *et al.*, 2009]. The SOFIE level 2 version 1.3 CH₄ is the target product being validated in this study.

Table 1 lists SOFIE CH₄ itemized errors based on the simulated retrieval responses to known error sources from 30 km up to the mesosphere at ~70 km. The CH₄ error analysis was performed by taking an original presumed unperturbed CH₄ profile, calculating the corresponding radiance profile using the forward model, and then perturbing the radiance profile by adding errors. Retrievals were then performed on the perturbed radiance profiles to obtain the CH₄ response. The SOFIE radiometer signals are digitized between 0 and 2¹⁵ (0–3 V) counts. Based on the 10⁵ SNR, the noise level is < 1 count. A 0.2-count noise level is used for the retrieval simulations to calculate the random error responses. The random error responses to the instrument noise are <1% below 50 km increasing to ~9% at ~70 km altitude. Systematic errors are contributed by several sources, including errors from applying the forward model, channel alignment uncertainty, removal of effects of interfering gases, temperature biases, and field-of-view drift on the Sun during the occultation event. Forward model error is partitioned between the BandPak forward model error and error due to spectroscopic parameters (3% line strength uncertainty). The error response from the forward model is the largest of all contributions, ~3% throughout the altitude range ~25–70 km. The interfering term refers to the error response to the 10% uncertainty of the interfering species (i.e., H₂O and O₃ vmrs). They are the in-band contributions not totally removed in the retrieval. The CH₄ in-band error below ~50 km is ~1–2%, and this reduces to a negligible level in the mesosphere. Alignment differences between the CH₄ channel and CO₂ channel fields of view (FOVs) due to registration of the density profile (or $T(P)$) with altitude will also impact the CH₄ retrieval. Assuming an alignment difference of ~100 m, the corresponding CH₄ error response is ~1.5% and remains rigorously conserved with height. Temperature bias errors must be accounted for since the retrieval of the gaseous products depends on temperature. SOFIE temperature bias becomes significant above ~40 km, varying between ~2 K and ~5 K in most cases and occasionally reaching ~10 K in the mesopause region [Stevens *et al.*, 2012]. Given a linearly increasing temperature bias of 0.5 K to 3 K in the vertical range ~40–70 km, the error response in CH₄ also linearly increases from ~0.4% at 50 km to 1.5% at 70 km. FOV drift on the Sun will result in a decrease in the measured intensity that would be falsely attributed to the atmosphere since the simulated transmissions are integrated spatially over the SOFIE FOV response

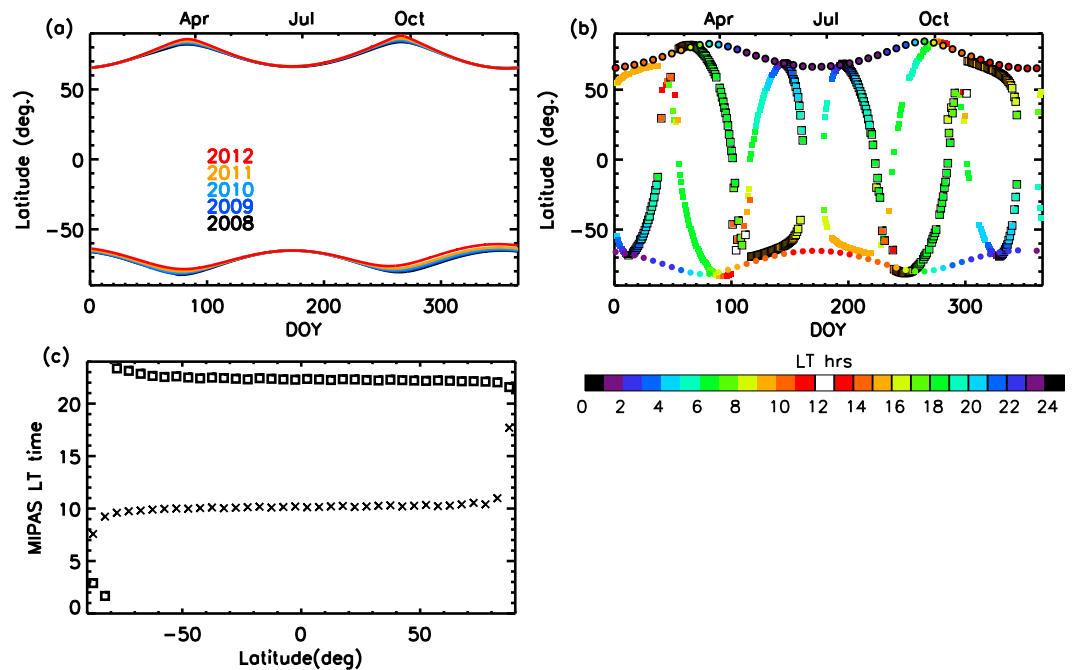


Figure 2. (a) SOFIE latitude coverages over years 2008–2012. (b) SOFIE 2009 (dots) and ACE (squares) latitude coverage overlaid to show how SOFIE and ACE coincide in terms of latitudes and local times. The symbols with black outlines are local times after 12:00 pm. (c) The MIPAS local time variation with latitude. The squares and crosses represent the ascending and descending nodes, respectively.

and the measured solar source function. The decrease of solar intensity away from Sun center is described by the solar limb darkening curve (SLDC). Signal drift caused by FOV movement is removed by adjusting incoming solar intensity using pointing information from the Sun sensor along with the SLDC. The CH₄ error induced by the inaccuracy of the removal process is ~1% at all altitudes.

The total modeled SOFIE systematic error remains at ~4% throughout the vertical range ~25–70 km. Since the random error is much smaller below ~50 km than at higher altitudes, the total error (root-sum-square of the random and systematic errors) remains at ~4% below ~50 km and then rapidly increases to ~10% at 70 km.

2.2. Correlative Data Sets

2.2.1. SCISAT ACE-FTS

The ACE-FTS instrument [Bernath *et al.*, 2005] is onboard the Canadian satellite mission SCISAT for remote sensing of minor species in Earth’s atmosphere using a solar occultation technique. It was launched into a low Earth circular Sun-synchronous orbit (altitude ~650 km, inclination 74°) on 12 August 2003. The ACE-FTS instrument, or ACE, as termed in the remainder of this paper, is a high spectral resolution (~0.02 cm⁻¹) Michelson interferometer operating in the medium-to-long infrared range from ~2.2 to ~13.3 μm (750–4400 cm⁻¹). Version 3.5 ACE data are used in this study. Like SOFIE, ACE obtains ~30 measurements per day, but the coverage spreads over the entire globe throughout a year. As a result, the polar region data coverage in ACE is much coarser than that provided by SOFIE. Figure 2a shows the ACE and SOFIE latitude coverages throughout a year. The colored symbols are data points in 2009 with the coloring representing the local time variation. Latitude and local time coincidences are in concert because both instruments take measurements at sunrise or sunset. These latitude coverages are roughly representative of years 2008–2012. ACE measures vertical profiles of temperature and a large number of trace gases including CH₄ in the stratosphere and mesosphere. More than 60 microwindows covering a range of 1245.14–2888.48 cm⁻¹ (~3.46–8.03 μm) are used to retrieve CH₄ over different altitude ranges [De Mazière *et al.*, 2008]. ACE has a good SNR (>100) and a FOV of ~1.25 mrad [Châteauneuf *et al.*, 2004; Bernath *et al.*, 2005] which is about twice as broad as the SOFIE FOV for the CH₄ channel (~0.6 mrad). The ACE vertical resolution is ~4 km from the cloud tops to ~150 km [Bernath *et al.*, 2005]. A validation study of ACE v2.2 CH₄ by De Mazière *et al.* [2008] indicates that ACE CH₄ vmrs are systematically smaller than the Envisat MIPAS CH₄ below ~20 km as well

as above ~60 km, but in between, the difference fluctuates within ~10–15% suggesting a good agreement. In the same paper it also showed that ACE CH₄ is ~5–20% larger than the UARS HALOE measured CH₄. A full error analysis based on the simulated responses to different error sources is not currently available for ACE CH₄. However, the inversion error, which can be described by the root-mean-square (RMS) of single-profile precisions, varies between ~2% and ~3% below ~60 km and increases to ~10% at ~70 km [e.g., *De Mazière et al.*, 2008]. *De Mazière et al.* [2008] also commented that spectroscopic uncertainty is the dominant error source in ACE CH₄ which leads to a systematic error of the order of ~20%.

2.2.2. Envisat MIPAS

Envisat was launched in 2002 with 10 instruments aboard, and the mission ended in April 2012. The satellite orbital track is in a near-circular, Sun-synchronous orbit at ~765 km altitude. The inclination angle is 98.3023° (near polar), and the equator crossing time for the descending node is 10:00 am. The Envisat track repeats the same local times (10:00 am/pm) each orbit, and therefore the local time coverage does not vary with day or year. Figure 2c shows the MIPAS local time variation with latitude, indicating that the latitudinal variation of local time is very small except for on the high polar latitudes. Under this latter condition, there is a rapid local time migration between the ascending and descending nodes.

The MIPAS instrument on the Envisat is a Fourier transform spectrometer for the detection of limb emission spectra in the middle and upper atmosphere. It observes the medium-to-long infrared spectral range from ~4.15 μm to ~14.6 μm with a full resolution of ~0.035 cm⁻¹ originally but a reduced resolution of 0.0625 cm⁻¹ since 2005. The MIPAS V6 data set used in this study covers the full MIPAS mission, including the full resolution phase (July 2002 to March 2004), test measurements performed in August to September 2004, and the reduced resolution phase (January 2005 to April 2012). MIPAS is able to detect and resolve a large number of emission features of atmospheric species. The MIPAS products include nitrogen dioxide (NO₂), nitrous oxide (N₂O), methane (CH₄), nitric acid (HNO₃), ozone (O₃), and water vapor (H₂O). MIPAS CH₄ microwindows for the reduced spectral resolution are in the range of 1228.4375–1236.8125 cm⁻¹ (8.14–8.08 μm) [<http://eodg.atm.ox.ac.uk/MIPAS/mw/>]. The MIPAS measurement and retrieval gives a vertical resolution of ~3 km below ~42 km altitude, whereas above this altitude the resolution degrades to ~5–8 km. The MIPAS SNR degrades rapidly from a few hundred to <10 from the lower to upper stratosphere [*Hoffmann et al.*, 2008]. This may partially explain the relatively large random errors (>20%) of MIPAS CH₄ (see section 3). The offline reprocessed V6 Level2 MIPAS data [*Raspollini et al.*, 2006; *Payan et al.*, 2009; *Engel et al.*, 2016] used in this study have a valid vertical range up to ~68–70 km that is slightly more extended than from the near-real-time retrievals [*Burgess et al.*, 2004]. MIPAS collects up to ~1400 events per day and provides daily global coverage. The Institut für Meteorologie und Klimaforschung, Karlsruhe/Instituto de Astrofísica de Andalucía, Granada (IMK/IAA) retrieved MIPAS CH₄ product has been validated against SOFIE [*Laeng et al.*, 2015] showing a mean difference of ~3–8% in the upper stratosphere to lower mesosphere.

The MIPAS offline error analysis is provided by the Oxford University group, and the current online version is available at <http://eodg.atm.ox.ac.uk/eodg/project/mipas/err/>. The error analysis is based on the theoretical framework detailed by *Dudhia et al.* [2002]. The random error is the propagation of instrument noise through the retrieval, and the systematic error is the root-sum-square of individual systematic error sources. These errors and the SOFIE errors provided in Table 1 will be used to calculate the combined errors shown in the following profile comparisons.

3. Coincidence Analysis

3.1. Strategies

In this section we examine the statistical moments of the near-coincidence pairs of profiles between SOFIE and ACE or SOFIE and MIPAS. The coincidences are searched in a spatial and temporal box of 20° longitude × 5° latitude × 2 h time. A smaller box is always preferred to minimize the differences caused by spatial or temporal variability. In this particular case the spatial dimensions are chosen based on the 15 orbits of satellite coverage. Two hours is a sufficiently confined time interval even if diurnal or semidiurnal variability is significant. We understand, however, that CH₄ does not show apparently photolysis caused day and night differences below ~70 km of altitude. Figure 3 shows the monthly variations of the coincidence number, indicating which months are used most in calculating the seasonal statistics. Figure 3a shows

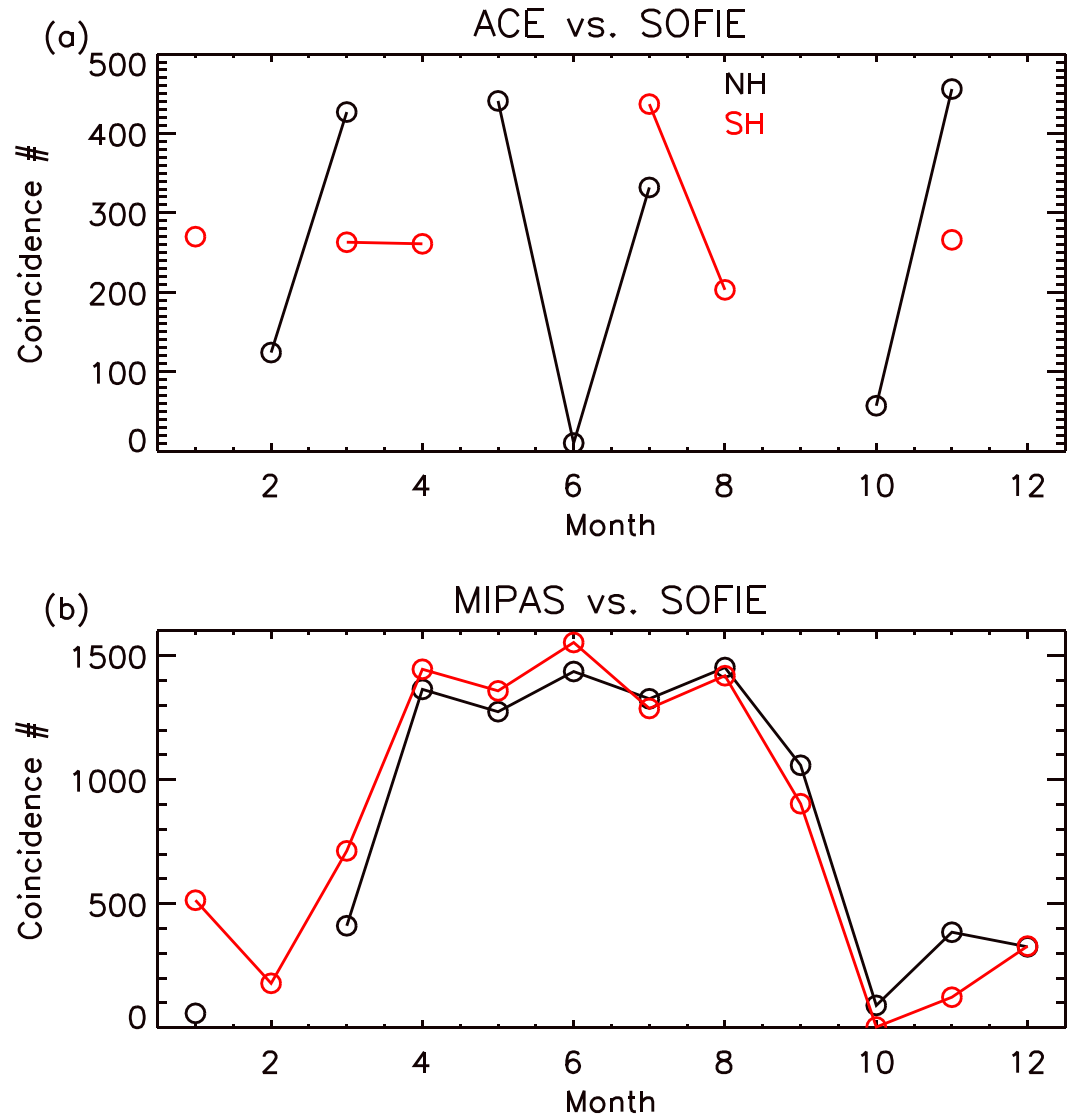


Figure 3. Monthly time series of number of coincident profiles between (a) SOFIE and ACE, and (b) SOFIE and MIPAS. The ACE comparisons are for years 2008–2012, and the MIPAS comparisons are for years 2008–2011. The universal coincidence box chosen is 20° in longitude, 5° in latitude, and 2 h in time.

the SOFIE versus ACE coincidences over full years from 2008 to 2012. The higher coincidence numbers correspond well with what Figure 2a has indicated about the latitude and local time coincidences. One exception is that in the NH in January there are no coincidences given the close latitude and time overlaps because the longitude differences fall out of the 20° interval during this time. Figure 3b shows SOFIE versus MIPAS coincidence numbers. Since MIPAS covers almost exclusively two local times (Figure 2c) while SOFIE local time coverage varies significantly throughout a year, it is not surprising that the high coincidence numbers occur primarily in the middle part of a year from April to September.

A vertical smoothing procedure is applied to each coincident profile with the higher resolution between the two data sets, to ensure that SOFIE and the correlative data sets are better matched in their vertical resolutions. SOFIE CH₄ is being smoothed in all cases because it has a higher resolution than both ACE and MIPAS. For each pair of coincidental profiles, the SOFIE profile is interpolated onto the grids of the corresponding ACE or MIPAS profile grids using the least squares smoothing method. After the vertical smoothing, all coincident pairs are interpolated onto a common grid system in order to calculate the statistical moments at consistent vertical levels. The vertical profiles from the two data sets are compared

on a pressure coordinate, and the common grids are generated based on the equal spacing of the log pressure values.

The variable of primary interest in the coincidence analysis is the CH₄ vmr difference of SOFIE and the correlative data set at given log pressure levels. The statistical moments for a given pressure level are the mean and the 1 σ standard deviation (STD) of the differences in percent, i.e., $\text{diff} = (\text{CH}_{4_sofie} - \text{CH}_{4_corr}) / (\text{CH}_{4_sofie} + \text{CH}_{4_corr}) * 2 * 100$. The standard error of the mean (SEM) difference is defined as the STD of differences divided by the square root of the number of coincidences, describing the statistical significance of the mean difference. The SEM goes to zero asymptotically when there are an increasing number of coincidences, indicating a high statistical significance of the mean difference. The combined systematic error shown in the following comparisons refers to the root-sum-square of the systematic errors provided by the individual data sets, and the SEM of the differences, described by formula $\text{error}_{com_sys} = \sqrt{\text{SEM}^2 + \text{error}_{sofie_sys}^2 + \text{error}_{corr_sys}^2}$.

The combined random error is in a similar form, i.e., $\text{error}_{com_ran} = \sqrt{\text{error}_{sofie_ran}^2 + \text{error}_{corr_ran}^2}$ [von Clarmann, 2006; Rong *et al.*, 2009]. It is worth noting that when the combined random error is calculated, the random error of the higher resolution data set, i.e., SOFIE in this case, will be reduced by a factor of \sqrt{n} where n is the ratio between the resolutions of the correlative data sets and SOFIE. The combined random or systematic error provides the approximate total uncertainty ranges to the mean difference (bias) or STD of the differences. To further interpret, the mean difference or STD of the differences is expected to stay within the $\pm \text{error}_{com_sys}$ or $\pm \text{error}_{com_ran}$. However, this is not always the case since imperfect coincidences, including the horizontal, temporal, and the vertical resolution mismatches, will induce unaccounted for variability which is seasonal dependent. The vertical smoothing procedure significantly reduces the errors resulting from the vertical resolution mismatch. The errors induced by imperfect coincidences are not provided by the individual data retrieval teams since they are dependent on the pair of data sets being used. In Rong *et al.* [2009] it suggested that the mean difference values between the two data sets are not dependent on the size of the spatial or temporal coincident box. But the STD values of the differences are somewhat larger when the coincident box is less restricted.

The coincidence analyses are performed for the NH and Southern Hemisphere (SH) separately and are divided into four seasonal groups, summer, winter, spring, and fall. The summer months include June, July, and August (JJA) in the NH and December, January, and February (DJF) in the SH, and it is opposite for winter. The rest of the months split between spring and fall. Seasonal groupings are performed because strong versus weak dynamics in different seasons may produce different vertical distributions and magnitudes in the bias or STD of the differences.

3.2. Statistics of the Coincidences

3.2.1. Winter Months

Figure 4 shows the SOFIE versus ACE or MIPAS comparisons over the winter months (DJF for NH and JJA for SH). For each pair of coincident profiles we apply a smoothing procedure (see section 3.1) to the SOFIE profiles to match the vertical resolution of ACE or MIPAS. SOFIE and the two correlative data sets have similar vertical resolutions of ~ 2 km and ~ 3 – 4 km, respectively.

The seasonal mean profiles and their 1 σ STD profiles are shown on the left side of each pair of panels. The STD in this case reflects the variability over a 3 month period. For each set of comparisons, i.e., between SOFIE and ACE, or SOFIE and MIPAS, the resemblance is strong throughout the entire vertical range in terms of both mean state and STD. In the NH above ~ 60 km, the ACE versus SOFIE coincidences show collectively much smaller CH₄ than the MIPAS versus SOFIE coincidences, due to the presence of strong descent in February (when the ACE/SOFIE coincidences occur) bringing low CH₄ air downward. This situation occurs because ACE NH coincidences cover only February. There is a rapid expansion of the STD toward the lower stratosphere reflecting a large variability in nearly all winter comparisons except for NH with ACE. The occasional large values in SOFIE CH₄ below ~ 28 km are very likely caused by polar stratospheric cloud (PSC) signal contamination that is not corrected. In the NH the bias level < 28 km is less severe, especially in the SOFIE and ACE comparisons. This is probably because in February the PSC signals are weak and only sporadically appear as compared to December and January [Spang *et al.*, 2005]. The bias in the SH is much larger, often exceeding 40%. It is, however, worth pointing out that although the PSC contamination of the signals is a highly probable cause, a further study is required to confirm this and to eventually correct the SOFIE CH₄ in this altitude range.

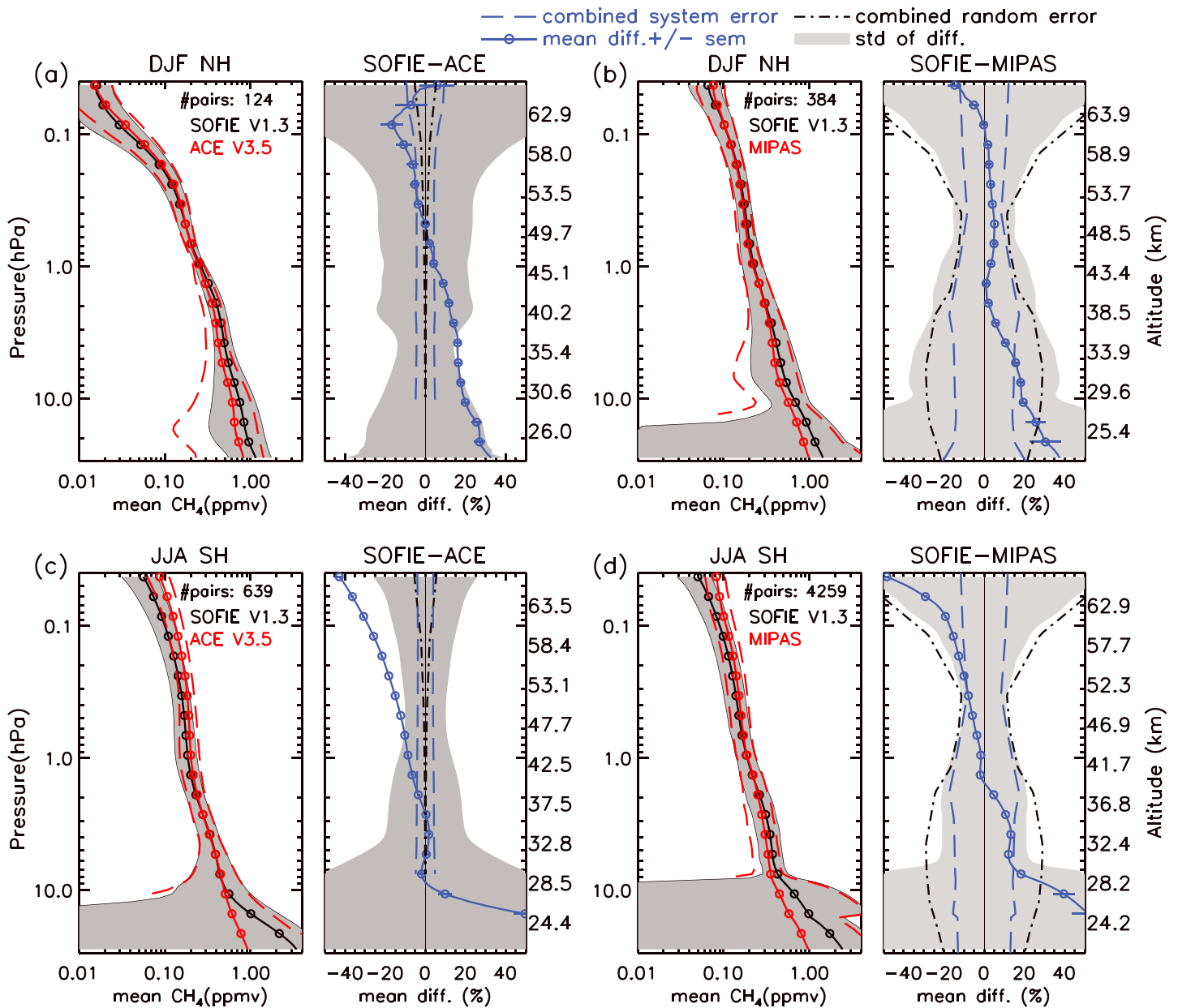


Figure 4. Statistical moments of the coincident CH₄ profiles between SOFIE and the two correlative data sets for the winter season. (a and c) SOFIE and ACE comparisons and (b and d) SOFIE and MIPAS comparisons. Figures 4a and 4b are for NH winter DJF, and Figures 4c and 4d are for SH winter JJA. For each of the four pairs of panels the left panel contains the mean values and the STD of all profiles, and the right panel shows mean difference values in percent (blue with circles) with the SEM bars, STD of the differences (gray shade), and combined systematic (blue dashed) and random errors (dash-dotted) from SOFIE and the correlative data set. In the ACE comparisons only SOFIE errors from Table 1 are shown. The SEM bars are extremely small in most cases because the coincident number is fairly large.

The mean and the 1σ STD of differences in percent and the combined errors are shown on the right side of each pair of panels. The rationales of presenting these curves are interpreted in section 3.1 above. The agreement between all three instruments is within 20% from ~ 28 – 30 km up to ~ 60 km except for the ACE JJA comparison in the SH where the $<20\%$ holds only up to ~ 50 km. In both ACE and MIPAS comparisons SOFIE has a high bias in the lower stratosphere and a low bias in the mesosphere. With respect to ACE, in the NH a high SOFIE bias dominates and persists below ~ 50 km, while in the SH a low SOFIE bias dominates and persists above ~ 35 km. Both high and low biases reach ~ 20 – 40% at the two ends of vertical range ~ 25 – 70 km, while in between the magnitude varies monotonically with altitude.

In the vertical range ~38–60 km, SOFIE and MIPAS mean difference values in the NH are within ~5%, while in the SH the SOFIE CH₄ is biased low relative to MIPAS by $\leq 20\%$ with a monotonic increase with height, suggesting a poorer agreement than in the NH. Below ~35 km in both hemispheres, the SOFIE CH₄ high bias relative to MIPAS reaches ~20–40%. In summary, the vertical distributions of SOFIE versus ACE and MIPAS mean difference values are roughly consistent, suggesting that an unknown but likely common mechanism has caused this.

In the MIPAS comparisons the STD of the differences above ~30 km agrees very well with the combined random errors except that in the SH (JJA) the combined random errors appear to be a few percent too conservative between ~30 km and ~40 km. The STD values below ~30 km far exceed the combined random errors, which is caused by the anomalously large CH₄ vmrs in SOFIE. The combined systematic errors also agree well with the mean difference values in the core region of ~30–70 km/30–52 km for the NH/SH. In the SH above ~52 km the SOFIE low biases exceed the combined systematic errors; in this case MIPAS and ACE comparisons show consistent results. The MIPAS error analysis was conducted by the Oxford University group [Dudhia *et al.*, 2002], and the errors for the polar winter condition are used in the current set of comparisons. In the ACE comparisons, on the other hand, only SOFIE random and systematic errors (see Table 1) rather than the combined errors are overplotted because a full error analysis for ACE CH₄ is not yet available currently, as is also mentioned above. Apparently, SOFIE systematic or random errors alone are too small to account for the mean difference or the STD of the differences.

3.2.2. Summer Months

Shown in Figure 5 are the summertime comparisons. Aside from the fact that the vertical distribution of the seasonal mean profiles agree well, we also note that the summertime variability is much smaller, reflected by the smaller STD values of CH₄ profiles. The vertical distribution of the mean difference is similar to the winter case, but the overall agreement is better. For example, the SOFIE and ACE CH₄ show a close agreement within ~5% in the vertical ranges ~45–65 km and ~40–60 km in the NH and SH, respectively. The SOFIE versus MIPAS mean difference values vary between plus and minus ~10% in the altitude range ~30–65 km, suggesting a fairly close agreement (in both hemispheres). It is also worth noting that in the short range of ~65–70 km the MIPAS mean profiles show abrupt variability, in opposite directions between the NH and SH, causing large biases relative to SOFIE. These features are present more than occasionally in the MIPAS data when the upper altitude limit (i.e., ~65 to 70 km) is approached. Since strong CH₄ variability is not expected in this altitude range, these features are most likely artifacts.

The STD values of the differences are generally much smaller in summer than in winter, reflecting a less disturbed state in summer. In the meantime, both the combined random and systematic errors in the MIPAS comparisons are also much smaller in summer than in winter below ~50 km, mainly due to the fact that the MIPAS errors for the polar summer condition are much smaller than those in the polar winter condition. Remember that only one universal set of SOFIE errors is provided. Below ~50 km the combined systematic and random errors both agree reasonably well with the mean and STD of the differences, whereas above ~50 km they are both too conservative.

3.2.3. Spring Months

In the NH spring the upper mesospheric CH₄ depletion (at ~70 km) usually lasts until mid-May. As a result, the mean profiles in the NH comparisons (Figures 6a and 6b) indicate small vmrs of ~0.02 ppmv at ~70 km. In the SH spring, on the other hand, the CH₄ depletion seems much less, characterized by consistently higher vmrs above ~45 km than in the NH or a “bulged” shape in the vertical distribution and a smaller STD level. The mean profile in the ACE SH comparisons (Figure 6c) shows particularly high CH₄ abundance when approaching ~70 km. This is because SOFIE and ACE coincidences in September–October–November (SON) mostly fall into November when the mesospheric CH₄ has recovered from the winter low vmrs.

Overall, the biases have shown a similar vertical distribution as in the previous results. The SOFIE low bias relative to ACE in the NH above ~50 km is within ~7%, while the high bias below ~50 km remains at ~10% down to ~30 km and then increases to ~20% at ~25 km. In the SH the SOFIE bias relative to ACE changes sign at ~40 km, and the magnitudes reach ~15–20% both above and below this altitude. The SOFIE and MIPAS mean difference values in the NH are within ~10% between ~30 km and ~65 km. In the SH the bias distribution resembles the ACE comparisons, but above ~65 km or below ~30 km the SOFIE high bias relative to MIPAS rapidly increases to ~40% or greater. In the MIPAS comparisons both combined systematic and random

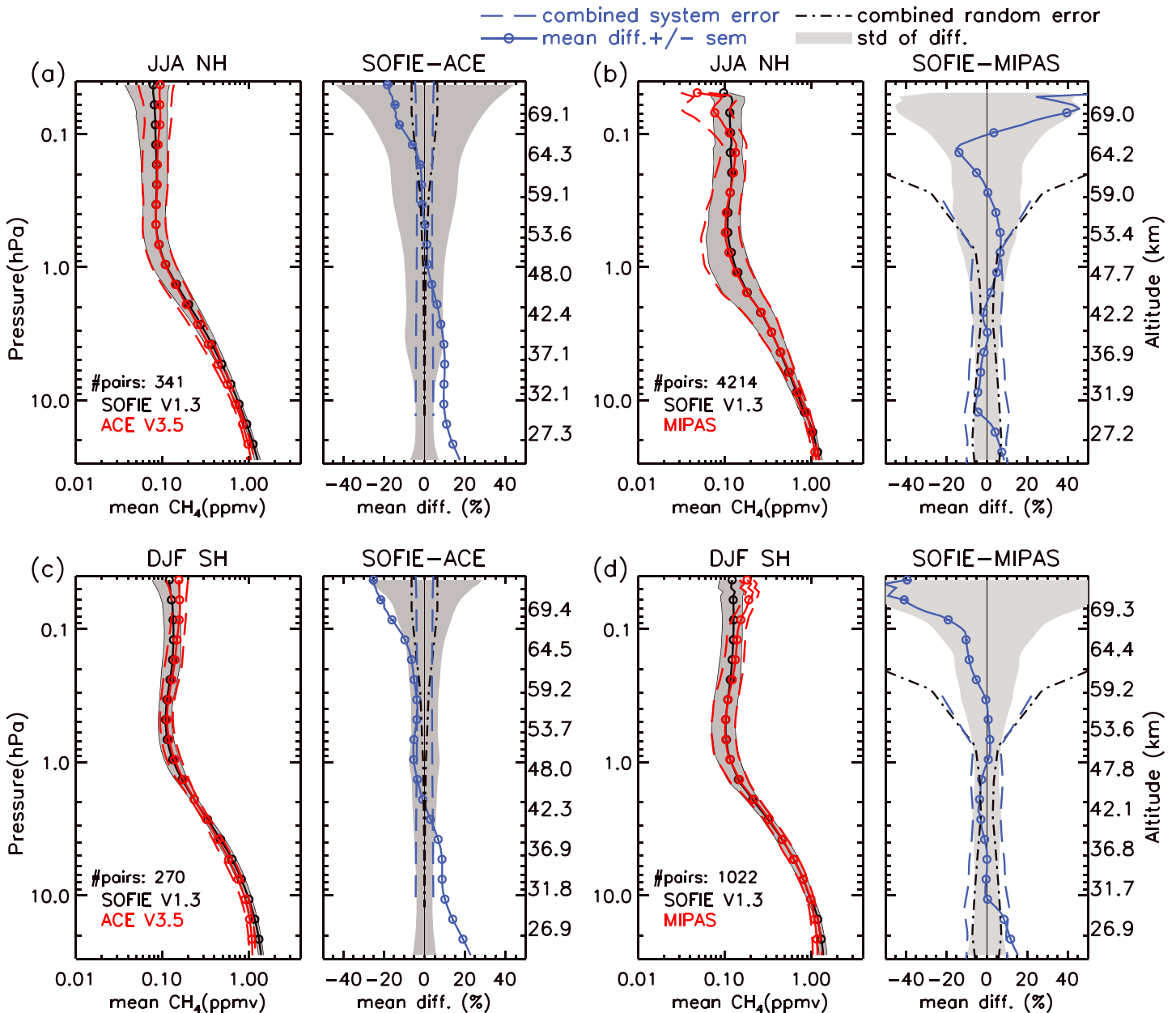


Figure 5. Same as Figure 4 except for the summer season. The blue dashed line stopped at ~60 km on the right panels because MIPAS systematic error value at ~68 km is not provided in the polar summer condition.

errors show reasonable agreement with the mean difference and the STD of the differences. Similar to winter and summer, MIPAS errors are occasionally more conservative in the core region between 30 km and 60 km, such as in the NH March–April–May (MAM) period. In the SH spring below ~28 km and above ~60 km the biases far exceed the combined systematic errors. We point out here that for both spring and fall comparisons the MIPAS global composite errors are adopted.

3.2.4. Fall Months

In fall, the seasonal mean profiles (Figure 7) exhibit striking agreement between the data sets with a majority of measurements showing a prominent depletion feature in the stratopause region. The height of this feature varies with month. For example, in the NH comparisons this depletion occurred at a lower altitude in ACE than in MIPAS because the numbers of SOFIE coincidences with the two data sets peaked at different months, i.e., November and September, respectively.

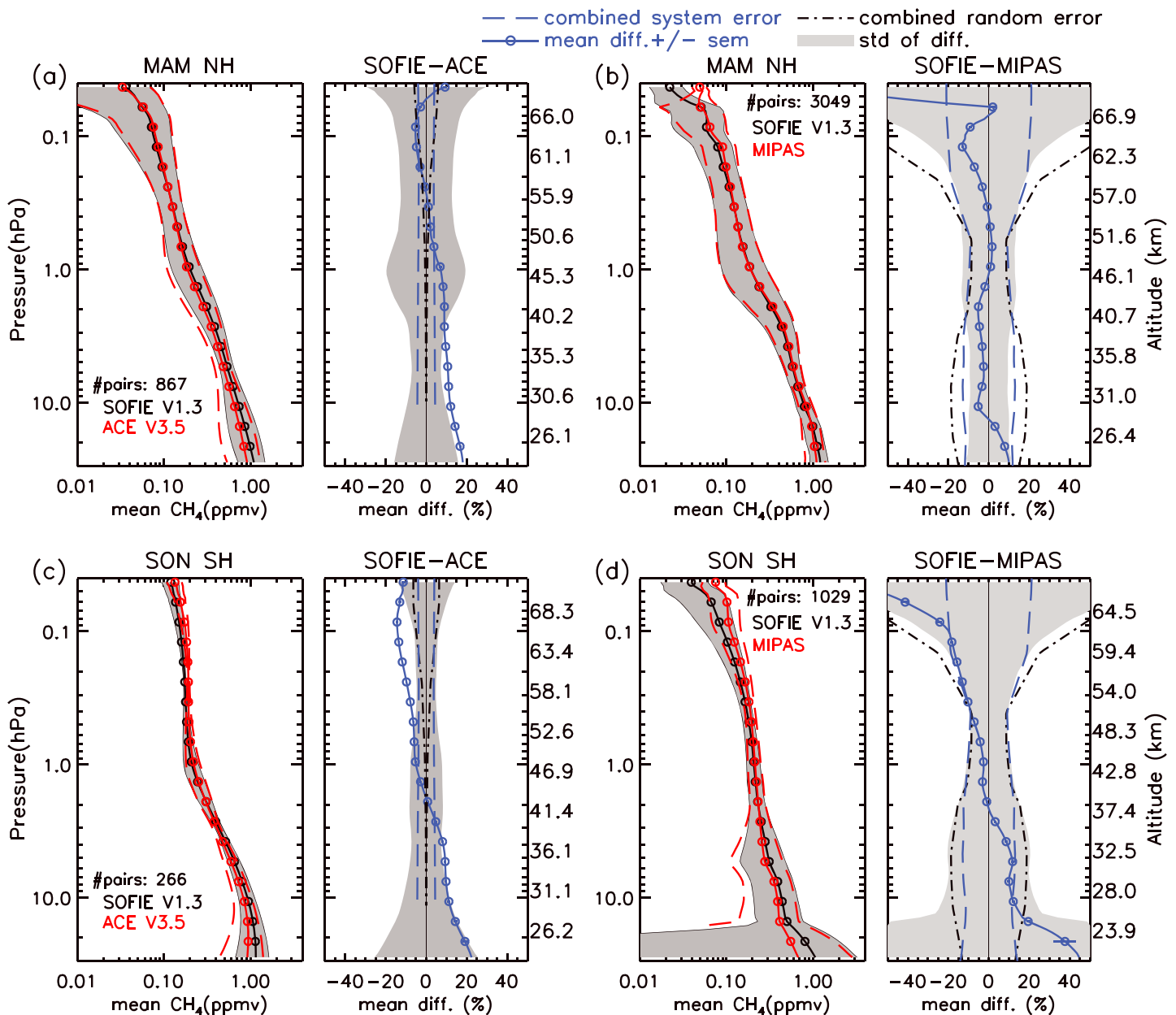


Figure 6. Same as Figure 4 except for the spring season.

In the NH, SOFIE and ACE mean difference values are within ~5% in the ~30–50 km altitude range. Above and below this range the bias increases to ~20% in both positive and negative directions. In the SH a close agreement of ~2% occurs between ~40 km and ~55 km, with a similar bias distribution above and below. However, the SOFIE high bias below ~40 km often reaches ~20% in the SH suggesting a somewhat poorer agreement than in the NH. SOFIE and MIPAS mean difference values in the NH are within ~8% in the vertical range ~30–65 km, suggesting a fairly close agreement over a much longer range. In the SH, SOFIE is biased high relative to MIPAS by ~2–15% below ~43 km and is biased low above. The negative bias above ~43 km increases to ~20% at ~60 km and further to ~40% or greater above ~60 km. In the MIPAS comparisons the mean difference values are mostly within the combined systematic errors. But the MIPAS random errors, which are the global composite as is mentioned above, do not capture the vertical distribution of the STD of the differences. In both ACE and MIPAS comparisons, the STD of the differences has a maximum characterized by a “bulge” in the upper stratosphere, which is very likely associated with the presence of the

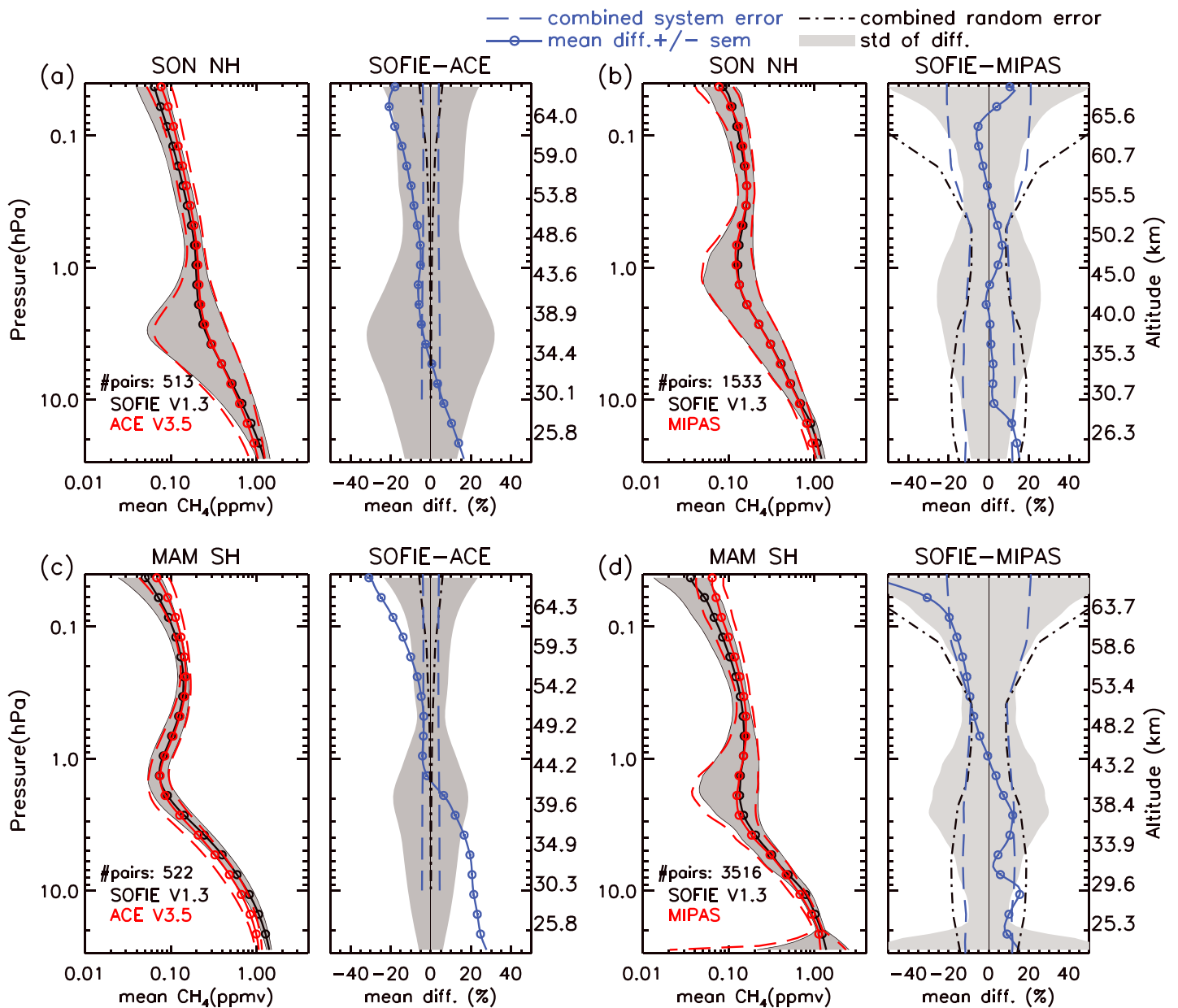


Figure 7. Same as Figure 4 except for the fall season.

rapidly descending depletion feature throughout the fall season (see the following section 4). Such a rapid variability will be reflected in the STD of the differences due to imperfect coincidences in space and time. As is mentioned above, errors due to the spatial and temporal mismatch are not accounted for in the error analyses provided by the individual data retrieval teams.

3.2.5. All Seasons Combined

Summarizing the comparisons, we conclude that qualitative agreement between SOFIE and ACE or MIPAS CH₄ is fairly close in terms of the seasonal mean climatology and intraseasonal variability. Table 2 shows the averages of the mean difference values over all seasons on a series of altitude levels from ~25 km to ~70 km for different hemispheres and data sets, respectively. SOFIE CH₄ is biased high in the stratosphere and biased low in the mesosphere by a varying percentage. SOFIE versus ACE and MIPAS CH₄ comparisons both support this conclusion. In the lower stratosphere a SOFIE high bias of ~20% is highly persistent. The all-season average indicates that the turning point of the bias from positive to negative occurs at

Table 2. The Numbers Outside and Inside the Parenthesis are Mean Percent Differences and the Uncertainties (1σ Standard Deviation of the Percent Differences), Respectively, Relative to SOFIE CH₄ for Different Data Sets, Hemispheres, and Altitudes^a

Data set/hemisphere	Altitude (km)									
	25 km	30 km	35 km	40 km	45 km	50 km	55 km	60 km	65 km	70 km
ACE NH	19.4 (6.6)	12.5 (5.8)	9.4 (6.6)	6.6 (8.0)	3.3 (6.7)	0.1 (3.9)	-3.0 (4.1)	-5.9 (4.5)	-13.0 (5.7)	0.6 (17.2)
ACE SH	40.7 (40.0)	13.1 (5.5)	9.4 (7.4)	4.2 (5.0)	-3.7 (2.0)	-6.3 (2.8)	-7.5 (4.9)	-11.4 (6.2)	-18.2 (7.1)	-26.8 (12.1)
MIPAS NH	16.5 (12.6)	3.8 (12.3)	3.1 (8.6)	0.1 (4.3)	0.6 (2.1)	5.0 (2.5)	2.4 (2.2)	-2.4 (3.7)	-3.4 (6.7)	-29.2 (38.4)
MIPAS SH	30.8 (28.2)	14.3 (13.7)	7.9 (5.7)	2.6 (5.7)	-1.1 (1.4)	-3.6 (3.2)	-8.1 (4.1)	-13.0 (3.0)	-22.8 (2.9)	-61.9 (7.3)
All cases combined	27.7 (26.1)	11.2 (11.1)	7.2 (6.9)	3.8 (6.0)	-0.2 (4.5)	-0.9 (5.1)	-4.0 (5.4)	-8.2 (5.8)	-12.9 (9.4)	-27.4 (29.4)

^aThe percent differences used are from Figures 5–8 shown in this paper. The same statistics for all cases combined are shown in the last row.

~55–60 km in the NH and ~40–45 km in the SH. This means that the negative bias in the NH takes up a much shorter range than in the SH. In the core region from ~30 km to ~65 km the mean difference values are generally smaller, varying between 0% and ~15%. The agreement in the NH is a few percent better. For example, SOFIE and MIPAS show close agreement in the NH within ~4% in the vertical range of ~30–65 km. In the lower stratosphere <25 km or mesosphere >60 km the biases rapidly increase in most cases, and especially in the SH it reaches larger percentages of ~40–60%. It is worth noting that in the SH winter, the large bias in the lower stratosphere can be interpreted as being caused by unaccounted for PSC contamination of the signals in the SOFIE data, although a further study is required to confirm the causes.

The last row of Table 2 shows the averages of all the previous rows, representing a mean bias regardless of data sets and hemispheres. The bias distribution is dominated by the SH condition because it is generally larger than in the NH. On average, in the core region from ~30 km to ~65 km, the mean difference values are within ~13% while at ~25 km and ~70 km they increase to ~27%.

4. Methane, H₂O, and 2CH₄ + H₂O Variability

4.1. Methane and H₂O in 2009

To understand the statistics of the coincident profiles shown above in the context of a CH₄ seasonal climatology and to further validate SOFIE CH₄ beyond the coincidence analysis, in this section we will examine the seasonal variation of CH₄ and H₂O balance at SOFIE latitudes over the course of a year. Figure 8 shows the altitude versus day-of-year cross sections of SOFIE and MIPAS CH₄ in 2009, with the Aura Microwave Limb Sounder (MLS) measured H₂O [Waters *et al.*, 2006; Lambert *et al.*, 2007] contours overlapped, to provide a general picture of the correlation between CH₄ and H₂O in the polar region. The year 2009 does not represent any averaged state. On the contrary, the overall CH₄ level in this year is anomalously low and its winter and spring dynamics is highly unique among the recent years. In this year the CH₄ variability effects caused by the NH vertical descent are prominently displayed during late winter to early spring, and these characteristics were successfully modeled and interpreted by Siskind *et al.* [2015]. A recent paper by Siskind *et al.* [2016] further suggested that the seasonal CH₄ climatology follows different regimes and the year 2009 represents a regime in which a strong winter to early spring descent (of low CH₄) and a less vigorous late spring breakup of the polar vortex (i.e., final warming) are combined. In contrast, if a vigorous final warming occurs, it will result in higher CH₄ being transported into the polar region. The other regimes will be revisited in the following section 4.2 of this paper.

Aura MLS H₂O is used because SOFIE H₂O is biased high by ~10–20% relative to both ACE and MLS [Rong *et al.*, 2010] in the vicinity of the stratopause where CH₄ conversion to H₂O is the strongest. The MLS is one of four instruments on the Aura satellite, launched on 15 July 2004. Aura is in a near-polar ~705 km altitude Sun-synchronous orbit, to give daily global coverage with ~15 orbits per day. MLS data products include a large number of atmospheric constituents, temperature, and tropospheric cloud ice. MLS version 4.2 H₂O is used in this study. The MLS vertical resolution is about ~3–6 km below ~55 km and degrades to ~6–11 km above. We disregard the fact that MLS and SOFIE local times [Waters *et al.*, 2006] achieve poor overlaps because H₂O variability in the stratosphere is not strongly dependent on the local times.

We first note that Figure 8 indicates remarkable agreement between SOFIE (a and c) and MIPAS (b and d) CH₄. Figures 8a and 8b show that the strongest CH₄ depletion in the NH mesosphere (at ~70 km) occurs in late February to early March. This is associated with the strong descent following an extended stratospheric

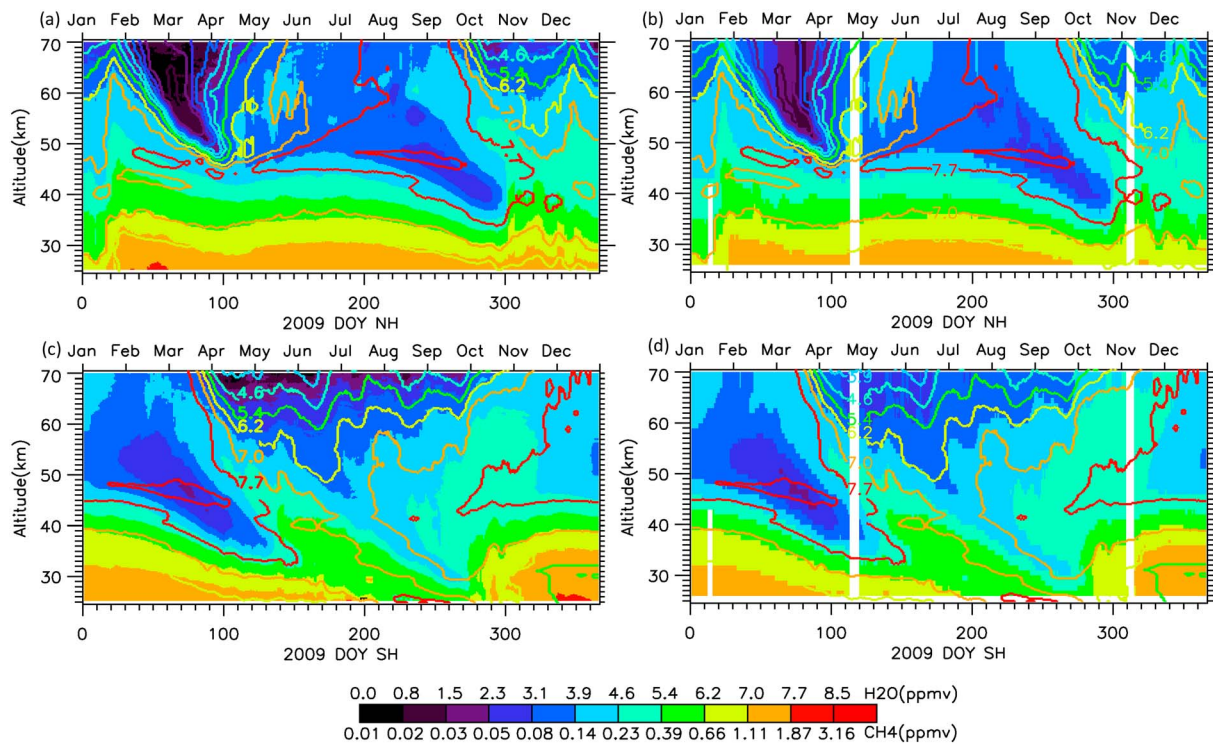


Figure 8. Altitude versus day-of-year (2009) cross sections of (a and c) SOFIE and (b and d) MIPAS CH₄. Both SOFIE and MIPAS CH₄ are overlaid by the MLS H₂O contours. Figures 8a and 8b are for the NH, and Figures 8c and 8d are for the SH.

warming and an elevated stratopause event that has received much attention in the literature [Randall et al., 2009; Manney et al., 2009]. A recent model/data comparison [Siskind et al., 2015] has shown values of CH₄ within this region to be as low as 0.01 ppmv. Water vapor shows a similar descent effect with very low values that are consistent with the source of the air mass well above ~70 km [Siskind et al., 2015]. In the upper mesosphere, there is strong conversion of both CH₄ and H₂O into H₂ or H [Le Texier et al., 1988]; thus, unlike the rest of the middle atmosphere, CH₄ and H₂O in the descent region are not anticorrelated. The CH₄ and H₂O depletion features narrow down and die out in early April at ~50 km or slightly lower altitude.

After a brief recovery of CH₄ in late May in the NH and a relatively prolonged recovery from October to November in the SH, in summer to early fall, we see a second region of decreasing CH₄ throughout the upper stratosphere to lower mesosphere, which in this case is clearly anticorrelated with H₂O. Such a seasonal difference in the CH₄ and H₂O relationship was also discussed in Remsberg et al. [1996] using HALOE data analysis. This indicates chemical conversion of CH₄ to H₂O [Le Texier et al., 1988; Brasseur and Solomon, 2005]. Upward transport lifts the large H₂O at the stratopause up into the mesosphere, as indicated by the yellow and red upward open contours during June–July in the NH and late November–December in the SH. The ascent appears to end in September in the NH and in March in the SH when both H₂O and CH₄ show the beginnings of descent. The oxidation of CH₄ at the stratopause ends as photochemical time constants become long with the diminished sunlight.

Figures 8c and 8d show the same cross sections in the SH, which share all the key features described above in terms of seasonal variability. Especially, the depletion from late summer to fall is very similar between the two hemispheres. This supports the current understanding that summer and fall are dynamically quiet and therefore the CH₄ distribution is primarily shaped by the chemistry. However, some noteworthy hemispheric differences do exist during winter and spring. For example, in the SH mesospheric descent is overall much weaker than in the NH, in which case extremely low CH₄ values do not occur below ~70 km. But the descent in the SH penetrates more deeply into the stratosphere, i.e., down to ~30 km. We can observe this, for example, by following the CH₄ depletion at a given altitude, as is indicated by the 0.14 ppmv contour marked by

the grayish blue shade. This was also seen in HALOE [Siskind *et al.*, 2000] and is because in the SH the descent remains uninterrupted by planetary wave mixing over a much longer period of time, i.e., since April. The polar vortex in the NH is highly variable interannually and intraseasonally and is generally driven by stronger wave forcing associated with the planetary wave breaking [McIntyre and Palmer, 1983]. Stronger wave forcing generally induces a more rapid descent and a stronger depletion, but when a major warming occurs the vortex will be disrupted and then be reformed. This would prevent a persistent descent throughout the NH winter and spring.

4.2. Yearly Differences From 2009

4.2.1. Rationale

Methane plays an important role in the total hydrogen budget, and $2\text{CH}_4 + \text{H}_2\text{O}$ is expected to be conserved vertically or across years if there are no net hydrogen sources or sinks. Figures 9, 10, and 12 show a set of altitude versus day-of-year maps. The variables shown are yearly differences of CH_4 , H_2O , and $2\text{CH}_4 + \text{H}_2\text{O}$ in 2008 (or 2011) with respect to 2009. SOFIE and MIPAS CH_4 , and MLS H_2O are used. MIPAS and MLS data are processed at a SOFIE latitude $\pm 1^\circ$ to calculate the daily zonal mean values. The actual variables shown in the figures are denoted by $\Delta\text{CH}_4|_{\text{yr}-2009}$, $\pm 0.5 \times \Delta\text{H}_2\text{O}|_{\text{yr}-2009}$, and $\Delta(\text{CH}_4 + 0.5 \times \text{H}_2\text{O})|_{\text{yr}-2009}$. A factor of 0.5 is applied to measure the total hydrogen budget in terms of CH_4 molecules.

Differences from a given year rather than absolute vmrs are used to remove the intervention from the mean seasonal cycle and to readily examine the hydrogen balance across years and the corresponding partitioning between CH_4 and H_2O variability. The year 2009 is chosen as the baseline because it is documented in the literature to have its characteristics widely known. We will later find in this paper that the overall CH_4 level in 2009 is the lowest among the recent years. We aim to examine the CH_4 level responding to the winter-to-spring dynamical conditions that are substantially different from 2009. Siskind *et al.* [2016] categorized four types of winter and spring conditions characterized by weak/strong major warming or descent and weak/strong final warmings. Different combinations eventually determine the CH_4 level throughout summer. The winter and early spring descent in 2008 is less strong than in 2009 and can somewhat be labeled as being normal, although there is not a consensus on how to define a normal year in terms of winter and spring descent. The year 2011 has anomalously high CH_4 throughout the year, resulting from the horizontal mixing caused by stronger planetary wave forcing when final warming occurred [Hu *et al.*, 2014; Siskind *et al.*, 2016]. Theoretically, if there is no apparent year-to-year increase or decrease of the $2\text{CH}_4 + \text{H}_2\text{O}$, then the H_2O deficit/increase and the CH_4 increase/deficit would achieve a constant ratio of 2.0. Deviation from 2.0 would suggest that there are other H_2O sources or sinks such as net conversion from H_2 . A ratio of 2.0 is equivalent to $2\text{CH}_4 + \text{H}_2\text{O}$ being conserved, either with altitude or across the years. We will later show that deviation from this ratio regularly occurs.

4.2.2. $2\text{CH}_4 + \text{H}_2\text{O}$ Variability With Altitude and Across Years

4.2.2.1. NH

Figures 9a and 9b show the NH CH_4 differences between 2008 and 2009, or $\Delta\text{CH}_4|_{2008-2009}$. We point out here that these maps do not go above 50 km to focus on the stratosphere where the CH_4 destruction chain reaction is the strongest. From the validation point of view, above 50 km CH_4 and H_2O both show larger percent differences between data sets; therefore, the results are more difficult to interpret. We first note from Figures 9a and 9b that SOFIE and MIPAS $\Delta\text{CH}_4|_{2008-2009}$ show excellent agreement within a difference of ~ 0.1 ppmv over a large fraction of the domain except for early winter during November when the differences between the two data sets reach ~ 0.2 ppmv. Such a high degree of agreement on the maps of yearly differences further lends us confidence on the accuracy of SOFIE CH_4 beyond the seasonal climatology. From March to October $\Delta\text{CH}_4|_{2008-2009}$ are positive and negative above and below ~ 35 km, respectively. The strongest negative $\Delta\text{CH}_4|_{2008-2009}$ occurred from February to early March below ~ 35 km, which precedes the strongest positive $\Delta\text{CH}_4|_{2008-2009}$ that occurred in late spring from middle March to May above ~ 35 km. The late spring condition prevails through summer and fall, although the magnitude is reduced. Siskind *et al.* [2016] argued that the upper stratosphere is dynamically quiet in summer and therefore CH_4 variability in summer is primarily driven by the winter and spring dynamics. Further down in fall, the positive $\Delta\text{CH}_4|_{2008-2009}$ descends slightly, and then in winter to early spring more rapid variability, or disturbances, erupted. The traveling nature of the winter disturbances in $\Delta\text{CH}_4|_{2008-2009}$ is not as clear as in their counterpart in the H_2O differences (i.e., $\Delta\text{H}_2\text{O}|_{2008-2009}$), as will be shown below.

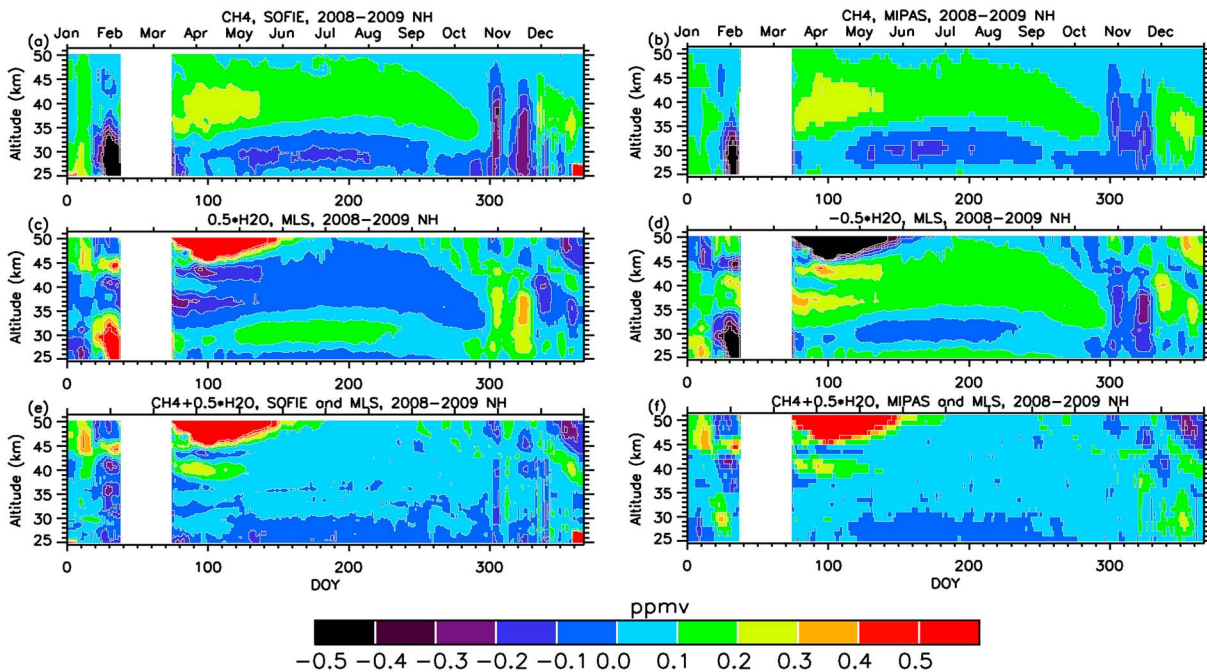


Figure 9. The 2008–2009 CH₄, H₂O, and the 2CH₄ + H₂O differences. (a and b) SOFIE and MIPAS CH₄. (c and d) MLS H₂O. The H₂O differences are halved in Figure 9c and then reversed in Figure 9d to make direct comparisons with the CH₄ differences. (e and f) The 2CH₄ + H₂O differences, which are also being halved.

Figures 9c and 9d show the NH $\Delta\text{H}_2\text{O}|_{2008-2009}$ being halved in positive and negative forms, respectively. The features in the maps of $\Delta\text{CH}_4|_{2008-2009}$ and $0.5 \times \Delta\text{H}_2\text{O}|_{2008-2009}$ are strongly anticorrelated, reflecting the condition that CH₄ and H₂O chemical conversion is the primary mechanism that controls the balance between the two constituents. If 2CH₄ + H₂O is conserved between 2008 and 2009, then $\Delta\text{CH}_4|_{2008-2009}$ and

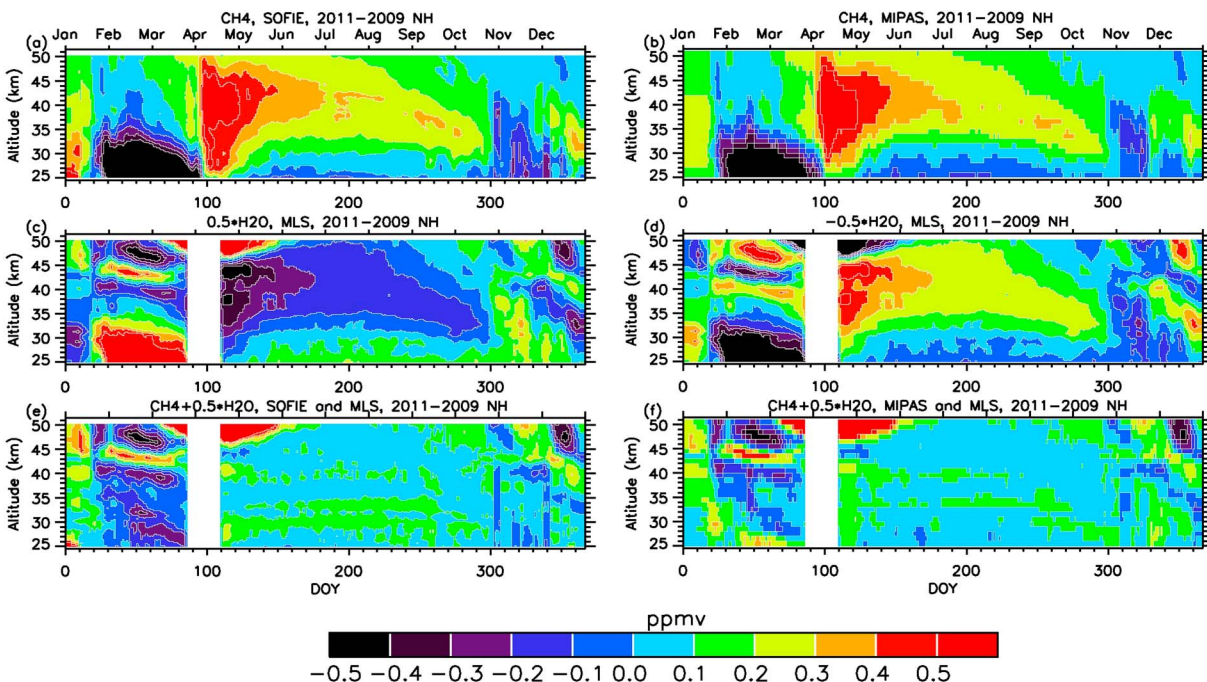


Figure 10. Same as Figure 9 except for the 2011 versus 2009 differences.

$-0.5 \times \Delta\text{H}_2\text{O}|_{2008-2009}$ will agree precisely, in which case $\Delta(\text{CH}_4 + 0.5 \times \text{H}_2\text{O})|_{2008-2009}$ (Figures 9e and 9f) will be consistently zero. Figures 9e and 9f indicate that $\Delta(\text{CH}_4 + 0.5 \times \text{H}_2\text{O})|_{2008-2009}$ is conserved to within $\sim \pm 0.1$ ppmv over a large fraction of the domain with respect to both altitude and day of year. During summer and fall the conservation is particularly great, reaching the highest altitude of the domain at ~ 50 km, whereas in winter and early spring it shows disturbances of a similar form in all the maps being presented suggesting a relatively poorly conserved state of $2\text{CH}_4 + \text{H}_2\text{O}$. Even in this later case $\Delta\text{CH}_4|_{2008-2009}$ and $0.5 \times \Delta\text{H}_2\text{O}|_{2008-2009}$ do still partially balance out below ~ 35 km, although the basic form of the oscillation is not eliminated in $\Delta(\text{CH}_4 + 0.5 \times \text{H}_2\text{O})|_{2008-2009}$. During wintertime in the stratosphere, active dynamics and lack of photolysis both contribute to disrupt the $2\text{CH}_4 + \text{H}_2\text{O}$ conservation. In addition, it is noteworthy that the winter disturbances are more distinct in the H_2O differences and appear to be traveling down with a period of ~ 1 month and a vertical wavelength of ~ 10 km throughout November and December. The largest offset in $\Delta(\text{CH}_4 + 0.5 \times \text{H}_2\text{O})|_{2008-2009}$ occurred in late spring throughout middle March to May above ~ 45 km. In this case the conservation breaks down completely due to the penetration of the low H_2O as well as low CH_4 air mass from above associated with the descent.

Shown in Figure 10 are similar maps except for between years 2011 and 2009. Methane is anomalously high throughout the entire year in 2011, which is ascribed to a vigorous final warming and the consequential “frozen-in” anticyclone with high CH_4 enclosed [Siskind *et al.*, 2016; Allen *et al.*, 2013]. The $\Delta\text{CH}_4|_{2011-2009}$ in the NH exhibits a pair of much stronger minimum and maximum features in late winter to spring as compared to 2008. Even though 2011 is more drastic, both 2011 and 2008 have $\Delta\text{CH}_4|_{\text{yr}-2009}$ in the same direction because in both years the winter and early spring descent is less strong than in 2009. In this case it is likely that both the deep and shallow branches of the meridional circulation [Dunkerton, 1978; Butchart, 2014] were weaker in 2011 (or 2008) than in 2009 resulting in a weaker descent in the mesosphere and meanwhile less poleward transport in the lower stratosphere. As in 2008, variables $\Delta\text{CH}_4|_{2011-2009}$ and $0.5 \times \Delta\text{H}_2\text{O}|_{2011-2009}$ balance out substantially but $\Delta(\text{CH}_4 + 0.5 \times \text{H}_2\text{O})|_{2011-2009}$ has shown greater deviation from zero, i.e., > 0.2 ppmv. The deviation is particularly strong and widespread in late spring April–May when $\Delta\text{CH}_4|_{2011-2009}$ maximizes. In this case the imbalance is a direct result of an anomalously large CH_4 increase but a smaller magnitude of H_2O deficit. If the total hydrogen remains constant between 2011 and 2009, then part of the CH_4 increase has to be balanced out by the H_2 deficit. Wrotny *et al.* [2010] examined the CH_4 and H_2O variability in the equatorial upper stratosphere over the years 1991–2005 and concluded that there is a H_2O gain of ~ 0.3 ppmv at the expense of a net H_2 loss. If in 2011 the low-latitude air has been vigorously transported into the polar region, then the insufficient H_2O deficit can be interpreted as the impact of excessive H_2O at the expense of H_2 in the lower latitudes. It is a plausible mechanism but would require a larger statistical set or modeling study which is beyond the scope of this paper.

In the vertical direction, both $\Delta(\text{CH}_4 + 0.5 \times \text{H}_2\text{O})|_{2011-2009}$ and $\Delta(\text{CH}_4 + 0.5 \times \text{H}_2\text{O})|_{2008-2009}$ indicate a similar degree of conservation with altitude throughout a year regardless of the fact that the CH_4 level in 2011 is much higher. It points to the conclusion that the degree of $2\text{CH}_4 + \text{H}_2\text{O}$ vertical conservation mainly follows a seasonal cycle, such as in summer and fall the conservation is to a better degree (± 0.1 ppmv) and holds up to higher altitude at ~ 50 km while in winter and spring it is relatively less conserved ($> \pm 0.2$ ppmv) and holds up to only ~ 35 – 40 km of altitude.

The above analysis showed that CH_4 variability (i.e., yearly differences) is the largest in the NH late spring time, and then it dwindles over summer. We will next find out whether the same finding applies to other years in a general sense. Figure 11 shows a scatterplot of the spring and summer relationship of $\Delta\text{CH}_4|_{\text{yr}-2009}$ using more years (2008–2014) of data. The horizontal axis is the late spring April or May monthly averaged $\Delta\text{CH}_4|_{\text{yr}-2009}$ depending on which month has the larger magnitude, and the vertical axis is the June–July–August averaged $\Delta\text{CH}_4|_{\text{yr}-2009}$. MIPAS data are also shown for years 2008, 2009, and 2011, which indicates a remarkable agreement with SOFIE in such a relationship. More years of SOFIE CH_4 are used to yield a quasi-linear relationship with a slope of ~ 0.5 between the late spring and summertime CH_4 variability. This supports the argument that summer CH_4 variability is driven by the spring dynamics. It is also noteworthy that 2009 turns out to be the year with the lowest CH_4 level among the seven years. Siskind *et al.* [2016] labeled 2008 and 2013 as both having an intermediate CH_4 level, although in 2008 there is a weak winter descent along with a weak final warming, while in 2013 it is opposite in both regards. In the current Figure 11 the years 2008 and 2013 also show a close agreement, confirming the results from Siskind *et al.* [2016]. The current analysis, however, is

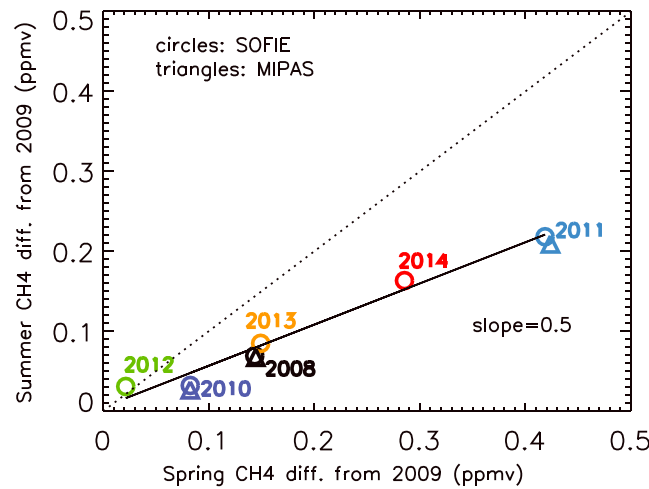


Figure 11. Late spring (April or May) versus summer (June–July–August) averaged CH₄ variability relative to 2009. The year 2009 is at the zero point (not shown). The calculations are based on the Figures 9 and 10 shown above except that more years up to 2014 are included for SOFIE. The altitude range used to calculate the averages is between 35 km and 50 km. The slope reflects how much the CH₄ variability, i.e., $\Delta\text{CH}_4|_{\text{yr}-2009}$, is reduced in summer from its late spring maximum.

not able to reflect the differences in the dynamics shown by *Siskind et al.* [2016] except for the fact that the largest late spring CH₄ variability occurs in April for 2008 whereas in May for 2013.

4.2.2.2. SH

Figure 12 shows the same cross sections as in Figure 10 except for the SH. We first point out that the magnitude of the SH differences are much smaller, which indicates that in the SH there is much weaker interannual variability. In the SH the SOFIE and MIPAS $\Delta\text{CH}_4|_{2011-2009}$ also show close agreement thereby serving as further SOFIE CH₄ validation. Even though the yearly differences in the SH are relatively weak, the winter disturbances are clearly present. The amplitude of these disturbances in $0.5 \times \Delta\text{H}_2\text{O}|_{2011-2009}$ reaches ~0.3–0.4 ppmv, which is slightly smaller but comparable to the amplitude in the NH. In the NH, late spring is the time

when yearly differences are the largest and then the established differences dwindle over summer and fall. But in the SH spring $\Delta\text{CH}_4|_{2011-2009}$ does not show any spring maximum, which makes the causes of the summer and fall features not as straightforward. The H₂O differences, i.e., $-0.5 \times \Delta\text{H}_2\text{O}|_{2011-2009}$, on the other hand, do somewhat maximize in late spring, but the features are not as sharp as in the NH and the overall magnitude is much smaller. What is also different from the NH is that in the SH starting from late summer in January, the pair of negative and positive $\Delta\text{CH}_4|_{2011-2009}$ in the lower and upper stratosphere move up systematically and positive differences take over the region below ~30 km altitude. Such a shift-up is also present in $-0.5 \times \Delta\text{H}_2\text{O}|_{2011-2009}$. In $\Delta(\text{CH}_4 + 0.5 \times \text{H}_2\text{O})|_{2011-2009}$ it also indicates a ~0.1–0.2 ppmv of increase across years, but the timing of occurrence is shifted toward summer and fall rather than in late spring as in the NH.

5. Conclusions

AIM SOFIE V1.3 CH₄ in the vertical range ~25–70 km is validated against ACE-FTS V3.5 CH₄ and Envisat MIPAS reprocessed V6 CH₄ in terms of statistics of coincident profiles, seasonal climatology, and balance between CH₄ and H₂O. Summarizing all profile comparisons, we conclude that SOFIE CH₄ shows overall qualitatively good agreement with the two correlative data sets in terms of the mean state and degree of variability for a large ensemble of profiles for a given season and hemisphere. The mean difference values indicate that SOFIE CH₄ is biased high by ~20% in the lower stratosphere and biased low by a similar percentage in the mesosphere close to the upper limit of the CH₄ data range at ~70 km. Throughout the altitude range from ~30 km to ~60 km, the agreement is much closer within a difference of ~15% or smaller. The biases are statistically significant in nearly all cases since several hundreds to thousands of coincident profiles are used, reflected by a negligibly small SEM. The mean difference and the STD of the differences are within the combined systematic and random errors in the MIPAS comparisons in most cases except around the lowermost limit <25 km or uppermost limit >65 km. The SOFIE systematic and random errors are much smaller than the counterparts provided by the MIPAS Oxford group. SOFIE CH₄ has some unaccounted for biases based on the comparison results. The smaller SOFIE random errors indicate that the noise level of the SOFIE profiles is much lower than that of the MIPAS profiles. The altitude of sign change for the SOFIE biases from positive to negative with respect to both ACE and MIPAS is at ~55–60 km in the NH and ~40–45 km in the SH. Agreement between SOFIE and the correlative data sets is overall better in the NH than in the SH. Agreement of SOFIE with MIPAS is overall better than with ACE. For example, in the NH SOFIE and MIPAS mean difference values stay within ~4% between ~30 km and ~65 km. Two anomalous situations are worth

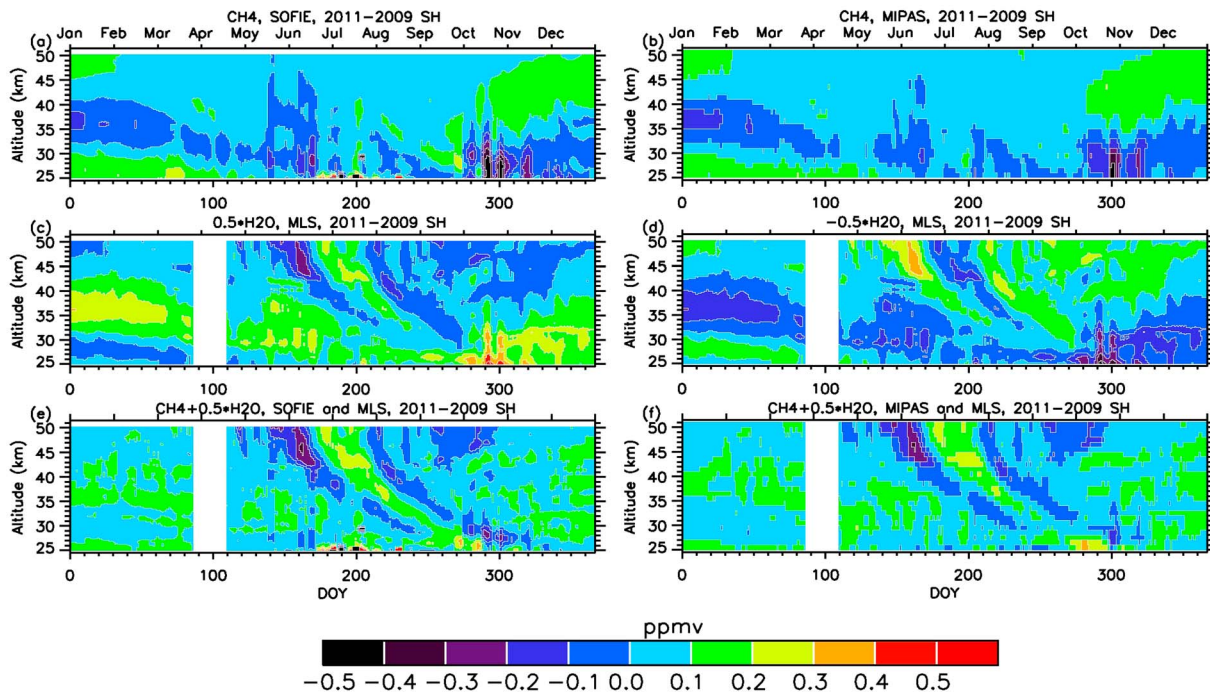


Figure 12. Same as Figure 10 except for the SH.

noting. First, below ~30 km SOFIE CH₄ occasionally reaches large values in winter, likely because PSC signals are not corrected, but this hypothesis needs to be further confirmed so that these errors can be corrected. Second, MIPAS CH₄ occasionally is anomalously large or exhibits abrupt variability when approaching ~70 km. Both conditions result in excessively large systematic differences (~40–60%) between SOFIE and MIPAS CH₄. In both cases, however, the sources of the biases are known to be limited in time and space so they are not pervasive enough to affect the overall data quality.

The polar CH₄ seasonal variability is shown in the altitude versus day-of-year maps centered at SOFIE latitudes daily. In such maps SOFIE and MIPAS CH₄ show remarkable agreement. In the polar winter to early spring, descent from the low CH₄ region above results in CH₄ depletion throughout the stratosphere and lower mesosphere. In the SH; however, the winter to early spring CH₄ depletion is much weaker. This is because planetary wave forcing is persistently stronger throughout winter and spring in the NH than in the SH. The second CH₄ decrease in summer and fall is primarily driven by chemical conversion to H₂O, characterized by highly consistent features between the NH and SH.

The CH₄ and H₂O yearly differences relative to 2009 (on a daily basis) reveal details of the polar 2CH₄ + H₂O balance over the course of a year, between years, and in the vertical direction. The H₂O difference is halved and reversed to make direct comparisons with the CH₄ difference. Doing so is to evaluate the deviation from the presumed 2CH₄ + H₂O conservation with altitude or across years. In these maps SOFIE and MIPAS CH₄ also show a close agreement supporting the SOFIE CH₄ accuracy beyond the seasonal climatology.

The vertical conservation of $\Delta(\text{CH}_4 + 0.5 \times \text{H}_2\text{O})_{\text{yr}-2009}$ holds up to ~50 km within ~0.1 ppmv in summer and fall, while in winter and early spring (~1 month period) disturbances occur in all the variables examined following the route of air descent. The residual fluctuations in $\Delta(\text{CH}_4 + 0.5 \times \text{H}_2\text{O})_{\text{yr}-2009}$ still reach an amplitude of ±0.2–0.3 ppmv, suggesting a poorer vertical conservation of 2CH₄ + H₂O. Further down in late spring, the conservation breaks down completely above ~45 km due to the downward penetration of the dry air mass associated with descent from the mesosphere.

Across the years, the main fractions of $\Delta\text{CH}_4_{\text{yr}-2009}$ and $0.5 \times \Delta\text{H}_2\text{O}_{\text{yr}-2009}$ balance out, but the residual (i.e., $\Delta(\text{CH}_4 + 0.5 \times \text{H}_2\text{O})_{\text{yr}-2009}$) shows an interannual variability. For example, in 2011 the CH₄ level is anomalously high; as a result, $\Delta(\text{CH}_4 + 0.5 \times \text{H}_2\text{O})_{2011-2009}$ has shown more consistent deviation from zero in the positive direction.

The largest CH₄ variability in the NH late spring (April or May) is a prominent feature. This maximum then dwindles over summer and fall. This condition is reflected by a linear relationship of the late spring versus summertime $\Delta\text{CH}_4|_{\text{yr}-2009}$, suggesting that summertime variability is about halved from its spring maximum for each given year from 2008 to 2014. The year 2009 is at the zero point because it has the lowest spring and summer CH₄ levels among all these years.

In the SH, the yearly differences are overall smaller. In addition, in the SH late spring, $\Delta\text{CH}_4|_{\text{yr}-2009}$ does not show any maximum, in which case the theory of spring control over summer on the CH₄ variability is not evidently supported as it is in the NH.

Acknowledgments

This work was accomplished at the Center for Atmospheric Sciences, Hampton University, Hampton, Virginia. Funding for the AIM mission was provided by NASA's Small Explorers Program under contract NASS-03132. SOFIE data are available at <http://sofie.gats-inc.com/sofie/index.php>. We thank the AIM and SOFIE/AIM team members for providing the SOFIE data, conducting error analyses, and sharing insights through science discussions. We appreciate the European Space Agency (ESA) for opening up a channel to obtain access to the MIPAS reprocessed data in a timely manner. We thank the ACE-FTS retrieval team for making the most recent V3.5 data available to us. The Atmospheric Chemistry Experiment (ACE) on the SCISAT platform is a Canadian-led mission mainly supported by the Canadian Space Agency and the Natural Sciences and Engineering Research Council of Canada. We are very grateful to the MLS/Aura data retrieval and science teams at JPL for making the MLS level 2 data available online for convenient download.

References

- Allen, D. R., A. R. Douglass, and S. E. Strahan (2013), The large-scale frozen-in anticyclone in the 2011 Arctic summer stratosphere, *J. Geophys. Res. Atmos.*, *118*, 2656–2672, doi:10.1002/jgrd.50256.
- Bailey, S. M., B. Thuraiajah, C. E. Randall, L. Holt, V. L. Harvey, D. E. Siskind, K. Venkataramani, M. E. Hervig, P. Rong, and J. M. Russell III (2014), A multi tracer analysis of thermosphere to stratosphere descent triggered by the 2013 Stratospheric Sudden Warming, *Geophys. Res. Lett.*, *41*, 5216–5222, doi:10.1002/2014GL059860.
- Bernath, P. F., et al. (2005), Atmospheric chemistry experiment (ACE): Mission overview, *Geophys. Res. Lett.*, *32*, L15S01, doi:10.1029/2005GL022386.
- Brasseur, G., and S. Solomon (2005), *Aeronomy of the Middle Atmosphere: Chemistry and Physics of the Stratosphere and Mesosphere*, 3rd ed., Springer, Dordrecht, Netherlands.
- Burgess, A., A. Dudhia, and C. Piccolo (2004), Intercomparison of MIPAS Near Real Time and Offline Data Products, paper presented at Second Workshop on the Atmospheric Chemistry Validation of Envisat (ACVE-2), ESA-ESRIN, Frascati, Italy, 3–7 May.
- Butchart, N. (2014), The Brewer–Dobson circulation, *Rev. Geophys.*, *52*, 157–184, doi:10.1002/2013RG000448.
- Châteauneuf, F., et al. (2004), On-orbit performance of the ACE-FTS Instrument, in *Earth Observing Systems IX, Proc. of SPIE*, vol. 5542, edited by W. L. Barnes and J. J. Butler, pp. 166–175, SPIE, Bellingham, Wash., doi:10.1117/12.559951.
- De Mazière, M., et al. (2008), Validation of ACE-FTS v2.2 methane profiles from the upper troposphere to the lower mesosphere, *Atmos. Chem. Phys.*, *8*, 2421–2435, doi:10.5194/acp-8-2421-2008.
- Dudhia, A., V. L. Jay, and C. D. Rodgers (2002), Microwindow selection for high-spectral-resolution sounders, *Appl. Opt.*, *41*, 3665–3673.
- Dunkerton, T. (1978), On the mean meridional mass motions of the stratosphere and mesosphere, *J. Atmos. Sci.*, *35*, 2325–2333, doi:10.1175/1520-0469(1978)035<2325:OTMMMM>2.0.CO;2.
- Engel, A., H. Bönisch, T. Schwarzenberger, H.-P. Haase, K. Grunow, J. Abalichin, and S. Sala (2016), Long-term validation of ESA operational retrieval (version 6.0) of MIPAS Envisat vertical profiles of methane, nitrous oxide, CFC11, and CFC12 using balloon-borne observations and trajectory matching, *Atmos. Meas. Tech.*, *9*, 1051–1062, doi:10.5194/amt-9-1051-2016.
- Funke, B., M. Lopez-Puertas, G. P. Stiller, and T. von Clarmann (2014), Mesospheric and stratospheric NO_y produced by energetic particle precipitation during 2002–2012, *J. Geophys. Res. Atmos.*, *119*, 4429–4446, doi:10.1002/2013JD021404.
- Gordley, L. L., et al. (2009), The solar occultation for ice experiment, *J. Atmos. Sol. Terr. Phys.*, *71*, 300–315, doi:10.1016/j.jastp.2008.07.012.
- Harries, J. E., S. Ruth, and J. M. Russell III (1996), On the distribution of mesospheric molecular hydrogen inferred from HALOE measurements of H₂O and CH₄, *Geophys. Res. Lett.*, *23*, 297–300, doi:10.1029/95GL03197.
- Hervig, M. E., L. L. Gordley, M. Stevens, J. M. Russell, S. Bailey, and G. Baumgarten (2009), Interpretation of SOFIE PMC measurements: Cloud identification and derivation of mass density, particle shape, and particle size, *J. Atmos. Sol. Terr. Phys.*, *71*, 316–330, doi:10.1016/j.jastp.2008.07.009.
- Hoffmann, L., M. Kaufmann, R. Spang, R. Müller, J. J. Remedios, D. P. Moore, C. M. Volk, T. von Clarmann, and M. Riese (2008), Envisat MIPAS measurements of CFC-11: Retrieval, validation, and climatology, *Atmos. Chem. Phys.*, *8*, 3671–3688.
- Howarth, R. W. (2015), Methane emissions and climatic warming risk from hydraulic fracturing and shale gas development: Implications for policy, *Energy Emiss. Control Technol.*, *3*, 45–54.
- Hu, J., R. Ren, and H. Xu (2014), Occurrence of winter stratospheric sudden warming events and the seasonal timing of spring stratospheric final warming, *J. Atmos. Sci.*, *71*, 2139–2134, doi:10.1175/JAS-D-13-0349.
- Laeng, A., et al. (2015), Validation of MIPAS IMK/IAA methane profiles, *Atmos. Meas. Tech.*, *8*, 5251–5261.
- Lambert, A., et al. (2007), Validation of the Aura Microwave Limb Sounder middle atmosphere water vapor and nitrous oxide measurements, *J. Geophys. Res.*, *112*, D24536, doi:10.1029/2007JD008724.
- Lashof, D. A., and D. R. Ahuja (1990), Relative contributions of greenhouse gas emissions to global warming, *Nature*, *344*, 529–531.
- Le Texier, H., S. Solomon, and R. R. Garcia (1988), The role of molecular hydrogen and methane oxidation in the water vapour budget of the stratosphere, *Q. J. R. Meteorol. Soc.*, *114*, 281–295.
- Manney, G. L., M. J. Schwartz, K. Krüger, M. L. Santee, S. Pawson, J. N. Lee, W. H. Daffer, R. A. Fuller, and N. J. Livesey (2009), Aura Microwave Limb Sounder observations of dynamics and transport during the record-breaking 2009 Arctic stratospheric major warming, *Geophys. Res. Lett.*, *36*, L12815, doi:10.1029/2009GL038586.
- Marshall, B. T., L. L. Gordley, and D. A. Chu (1994), BANDPAK algorithms for modeling broadband transmission and radiance, *J. Quant. Spectrosc. Radiat. Transfer*, *52*, 581–599, doi:10.1016/0022-4073(94)90026-4.
- McClintock, W. E., D. W. Rusch, G. E. Thomas, A. W. Merkel, M. R. Lankton, V. A. Drake, S. M. Bailey, and J. M. Russell III (2009), The cloud imaging and particle size experiment on the aeronomy of ice in the mesosphere mission: Instrument concept, design, calibration, and on-orbit performance, *J. Atmos. Sol. Terr. Phys.*, *71*, 340–355, doi:10.1016/j.jastp.2008.10.011.
- McIntyre, M. E., and T. N. Palmer (1983), Breaking planetary waves in the stratosphere, *Nature*, *305*, 593–600.
- Minschwaner, K., and G. L. Manney (2014), Derived methane in the stratosphere and lower mesosphere from Aura Microwave Limb Sounder measurements of nitrous oxide, water vapor, and carbon monoxide, *J. Atmos. Chem.*, *71*, 253–267, doi:10.1007/s10874-015-9299-z.
- Payan, S., et al. (2009), Validation of version-4.61 methane and nitrous oxide observed by MIPAS, *Atmos. Chem. Phys.*, *9*, 413–442, doi:10.5194/acp-9-413-2009.
- Randall, C. E., et al. (2005), Stratospheric effects of energetic particle precipitation in 2003–2004, *Geophys. Res. Lett.*, *32*, L05802, doi:10.1029/2004GL022003.

- Randall, C. E., V. L. Harvey, D. E. Siskind, J. France, P. F. Bernath, C. D. Boone, and K. A. Walker (2009), NO_x descent in the Arctic middle atmosphere in early 2009, *Geophys. Res. Lett.*, *36*, L18811, doi:10.1029/2009GL039706.
- Raspollini, P., et al. (2006), MIPAS level 2 operational analysis, *Atmos. Chem. Phys.*, *6*, 5605–5630.
- Remsberg, E. E., P. P. Bhatt, and J. M. Russell III (1996), Estimates of the vapor budget of the stratosphere from UARS HALOE data, *J. Geophys. Res.*, *101*, 6749–6766, doi:10.1029/95JD03858.
- Remsberg, E. E., et al. (2008), Assessment of the quality of the version 1.07 temperature versus pressure profiles of the middle atmosphere from TIMED/SABER, *J. Geophys. Res.*, *113*, D17101, doi:10.1029/2008JD010013.
- Rong, P., J. M. Russell III, L. Gordley, M. Hervig, L. Deaver, D. Siskind, P. Bernath, and K. A. Walker (2010), Validation of v1.022 mesospheric water vapor observed by the SOFIE instrument onboard the AIM satellite, *J. Geophys. Res.*, *115*, D24314, doi:10.1029/2010JD014269.
- Rong, P. P., J. M. Russell III, M. G. Mlynczak, E. E. Remsberg, B. T. Marshall, L. L. Gordley, and M. López-Puertas (2009), Validation of Thermosphere Ionosphere Mesosphere Energetics and Dynamics/Sounding of the Atmosphere using Broadband Emission Radiometry (TIMED/SABER) v1.07 ozone at 9.6 μm in altitude range 15–70 km, *J. Geophys. Res.*, *114*, D04306, doi:10.1029/2008JD010073.
- Russell, J. M., III, L. L. Gordley, J. H. Park, S. R. Drayson, D. H. Hesketh, R. J. Cicerone, A. F. Tuck, J. E. Frederick, J. E. Harries, and P. Crutzen (1993), The halogen occultation experiment, *J. Geophys. Res.*, *98*, 10,777–10,797, doi:10.1029/93JD00799.
- Russell, J. M., III, et al. (2009), The Aeronomy of Ice in the Mesosphere (AIM) mission: Overview and early science results, *J. Atmos. Sol. Terr. Phys.*, *71*(3–4), 289–299, doi:10.1016/j.jastp.2008.08.011.
- Siskind, D. E., G. E. Nedoluha, C. E. Randall, M. Fromm, and J. M. Russell III (2000), An assessment of Southern Hemisphere stratospheric NO_x enhancements due to transport from the upper atmosphere, *Geophys. Res. Lett.*, *27*, 329–332, doi:10.1029/1999GL010940.
- Siskind, D. E., F. Sassi, C. E. Randall, V. L. Harvey, M. E. Hervig, and S. M. Bailey (2015), Is a high-altitude meteorological analysis necessary to simulate thermosphere-stratosphere coupling?, *Geophys. Res. Lett.*, *42*, 8225–8230, doi:10.1002/2015GL065838.
- Siskind, D. E., et al. (2016), Persistence of upper stratospheric winter time tracer variability into the Arctic spring and summer, *Atmos. Chem. Phys. Discuss.*, doi:10.5194/acp-2015-1037.
- Spang, R., J. J. Remedios, L. J. Kramer, L. R. Poole, M. D. Fromm, M. Müller, G. Baumgarten, and P. Konopka (2005), Polar stratospheric cloud observations by MIPAS on Envisat: Detection method, validation and analysis of the Northern Hemisphere winter 2002/2003, *Atmos. Chem. Phys.*, *5*, 679–692.
- Stevens, M. H., L. E. Deaver, M. E. Hervig, J. M. Russell III, D. E. Siskind, P. E. Sheese, E. J. Llewellyn, R. L. Gattinger, J. Höffner, and B. T. Marshall (2012), Validation of upper mesospheric and lower thermospheric temperatures measured by the Solar Occultation for Ice Experiment, *J. Geophys. Res.*, *117*, D16304, doi:10.1029/2012JD017689.
- Summers, M. E., D. E. Siskind, J. T. Bacmeister, R. R. Conway, S. E. Zasadil, and D. F. Strobel (1997), Seasonal variation of middle atmospheric CH₄ and H₂O with a new chemical-dynamical model, *J. Geophys. Res.*, *102*, 3503–3526, doi:10.1029/96JD02971.
- von Clarmann, T. (2006), Validation of remotely sensed profiles of atmospheric state variables: Strategies and terminology, *Atmos. Chem. Phys.*, *6*, 4311–4320.
- Waters, J. W., et al. (2006), The Earth Observing System Microwave Limb Sounder (EOS MLS) on the Aura satellite, *IEEE Trans. Geosci. Remote Sens.*, *44*, 1075–1092.
- Wrotny, J. E., G. E. Nedoluha, C. Boone, G. P. Stiller, and J. P. McCormack (2010), Total hydrogen budget of the equatorial upper stratosphere, *J. Geophys. Res.*, *115*, D04302, doi:10.1029/2009JD012135.